Doctoral Dissertation

Plasmonic Enhancement and Quenching in Tip-Enhanced Fluorescence Microscopy

Jun Yu

December 2012

Graduate School of Engineering,
Osaka University

Plasmonic Enhancement and Quenching in Tip-Enhanced Fluorescence Microscopy

JUN YU

Abstract

Fluorescence is the emission of light by a substance that has absorbed light or some other type of energy. Practically, it occurs when electrons of a substance relax to their ground state after being excited to a higher electronic state by commonly absorbing light. One important application of fluorescence is optical microscopy. Fluorescence microscopy uses fluorescence instead of reflection or absorption to image a sample. In pursuit of high-resolution fluorescence imaging beyond diffraction limit, tip-enhanced fluorescence microscopy has been developed in the last decade. The concept of this tip-enhanced fluorescence is based on the fluorescence excitation by the enhanced light field localized at the apex of a metallic nanotip. The enhanced light field is originated from the resonance of abundant electron oscillations that are so-called surface plasmons. The resonance of surface plasmons can be excited by laser irradiation to a nanometer-sized metallic tip at a resonant wavelength. If a sample is placed close to the tip to get excitation by the enhanced light field, fluorescence can be greatly enhanced. This leads to tip-enhanced fluorescence. The enhanced light field is extremely confined and its strength decreases exponentially as a function of distance from the metal surface. Hence, the effect of tip enhancement on fluorescence is dependent on tip-sample separation. In other words, the smaller tip-sample separation is, the larger fluorescence is enhanced. However, besides enhancement there is the other phenomenon known as quenching occurring to diminish fluorescence. Quenching happens when the metallic nanotip gets very close to or mostly in contact with a sample. The excited electrons in the sample supposed to relax through fluorescence emission can instantly transfer their energy to the metal surface. In contrast to the effect of tip enhancement, fluorescence is diminished more by the effect of tip quenching as tip-sample separation goes smaller. Therefore, there are two competing processes affecting fluorescence when a metallic nanotip is induced to a fluorescent sample. As a result of tip-sample separation dependent fluorescence from effects of both enhancement and quenching, the strongest strength of fluorescence exists at a specific tip-sample separation. It is so significant to find out this specific tip-sample separation to get the optimization of enhancement and quenching as well as to get the strongest fluorescence intensity for high quality imaging. Till now, many studies have been done to decrease quenching effect by maintaining a

constant separation between tip and sample through many kinds of methods. However, the tip-sample separation is not so accurate to get the strongest strength of fluorescence. Many times the effect of enhancement compromises the effect of quenching through the tip-sample separation.

In this dissertation, I study the plasmonic enhancement and quenching in tip-enhanced fluorescence by developing a new technique of dynamically controlling tip-sample separation. The tip-sample separation dependent fluorescence intensity is observed and indicates an optimized separation preferred for fluorescence imaging.

The technique for dynamic control of tip-sample separation is developed from a tapping-mode atomic force microscope (AFM). As a tip oscillates sinusoidally in tapping-mode AFM, tip-sample separation varies dynamically with oscillation time. Through the synchronization of tapping oscillation and photon detection, the variation of optical signal as a function of tip-sample separation can be recorded. A multichannel photon counter is utilized to divide tip-sample separation and records optical signals corresponding to each divided tip-sample separations. As a consequence, tip-sample separation dependent optical signals can be recorded. The highest accuracy for tip-sample separation reaches 0.3 nm.

The application of this tip-sample separation control to tip-enhanced Raman scattering microscopy is demonstrated. Tip-sample separation dependent enhanced Raman scattering intensity is successfully detected, which indicates the enhancement of light field produced at the tip apex. In addition, this technique shows an advantage of detecting both far-field and near-field Raman signals in the tip-sample separation dependent Raman intensity. Thus in situ far-field subtraction can be carried out in one time measurement. Experimentally, Raman images of single-walled carbon nanotubes without far-field signal are achieved with a spatial resolution of less than 12 nm by means of raster-scanning the sample stage.

The effects of enhancement and quenching on fluorescent sample are implemented by measuring tip-sample separation dependent fluorescent intensity from quantum dots. Through tip-sample separation control, tip-sample separation dependent enhancement

and quenching of fluorescence intensity is successfully detected, and it obviously indicates an optimized tip-sample separation. At this optimized tip-sample separation, by means of the raster-scanning method, tip-enhanced fluorescence nano-images are constructed through the fluorescence intensity, indicating a high-quality fluorescence image with enhanced signal.

Keywords: tip-enhanced fluorescence, nano-imaging, plasmonic enhancement, quenching

Contents

Chapter 1.
Introduction

Tip-enhanced fluorescence microscopy is characterized with a capability of high-resolution far beyond the diffraction limit by means of utilizing a metallic nanotip. However, when the metallic nanotip is used to perform enhancement of fluorescence signal, fluorescence can be easily quenched due to energy transfer. The study of enhancement and quenching on fluorescence induced by a metallic nanotip results two completely opposite variations of strength as a function of the tip-sample separation. As a consequence, an optimized tip-sample separation can be indicated from the tip-sample separation dependent fluorescence intensity. The purpose of this study is to achieve tip-enhanced fluorescence microscopy at the optimized tip-sample separation that gives the best quality for fluorescence imaging. In this Chapter, I introduce the existing research and the present situation of studies in the related fields such as the scanning probe microscopy and diffraction limit, the plasmonics, the near-field optics and the tip-enhanced optical microscopy. The outline of this dissertation is described afterward.

1.1 Scanning probe microscopy and diffraction limit

In pursuit of detecting and observing biological cells and molecules in micrometer or nanometer scale, new imaging techniques with high spatial resolution are essential. In fact, imaging resolution has been improved very much since scanning probe microscopy (SPM) such as scanning tunneling microscopy (STM)[1] and atomic force microscopy (AFM)[2] was invented and developed more than 2 decades ago. A sharp tip with a radius of 10 to 20 nanometers is commonly used to raster scan over a sample in SPM. The

height information of samples is collected in SPM. Topographically, the resolution of image is determined by the diameter of the tip. In principle, SPM can achieve atomic resolution. Recently, sub-molecular resolution has been achieved with the development of SPM by an atomic functionalization of the sensor (that is the placing of a well-defined atom of molecule at the tip apex).[3]

Ever since SPM becomes so amazing to help us view the topographical structure of the material at atomic resolution, there is still an imperfection left that it cannot observe optical information referring to physical and chemical properties of the material. Optical information usually helps us to identify materials. In nature, most of substances exhibit physical and chemical properties responding to visible light. Because the visible light carries an energy that is comparable to the intrinsic electronic band gap energies of most of the naturally existing materials. This allows light to actively interact with substances at electronic energy level and then carry the information related to their physical and chemical properties.[4] As a matter of fact, optical imaging is the direct way to reveal these important optical information. However, traditional optics tells us that there is a diffraction limit for optical imaging. This is due to the wave nature of light. Ernst Abbe discovered this diffraction limit in 1873,[5] which is recognized to be roughly half of light wavelength. For example, with cyan light of 488 nm the diffraction limit is about 244 nm. Thus in a traditional optical microscope, two objects with a separation much smaller than half of light wavelength cannot be distinguished. However, most nano-structures or biological cells that have been under plenty of studies are smaller than 100 nm or even more. To observe them and understand their properties spectroscopically, an optical microscope needs to break through the diffraction limit.

1.2 Plasmonics

So how to obtain a sub-diffraction-limit resolution image or to realize nano-imaging in optical microscopy? A new field developed in the last decade gives a solution to achieve this purpose, it is now named as plasmonics. Plasmonics refers to the optical nano-science in the range limited to near-UV, visible and near-IR regions. It is closely related to the light-metal interactions. The light-metal interaction in nanometer scale

produces a new type of quantum known as surface plasmon polaritons (SPPs). In recent decades, it has been demonstrated that SPPs have the power to circumvent the diffraction limit.[6, 7] SPPs are electromagnetic waves that exist on the metal surface. In practice, they are results coupled from light field and collective oscillations of free electrons on the metal surface. Because of their high relation with free electron oscillations, SPPs cannot propagate away from the metal surface. Thus they are evanescent light waves. One of the most attractive aspects of SPPs is that they have much shorter wavelength than propagating light.[4, 8] In other words, if a SPP is used as a light source in optical microscopy, a sub-diffraction-limit resolution optical image can be obtainable. Another important aspect of SPPs is that they can work at a localized mode in resonance. Imaging a metal nanostructure excited by an external light field, SPPs are inherently confined to the surface of the metal nanostucture. When electrons oscillate along with the external light field at the same frequency, a resonant state of SPPs can be created; finally highly localized SPPs are produced. These resonantly localized surface plasmons have a greatly enhanced light field. It can act to excite biological molecules to get enhanced optical signals. Indeed, many new techniques have been developed based on this localized surface plasmon resonance (LSPR) to probe weak Raman scattering signal or fluorescence from a single molecule.[9, 10] With its especial properties of confinement and enhancement, LSPR has become an attractive method for optical spectroscopy and imaging.

1.3 Near-field optical microscopy

The enhanced field produced by LSPR is evanescent as a result of confined free electron oscillations. Its strength decreases exponentially as the distance from metal surface increases. This confined field region is so-called near field. Thus the non-propagating light in this region is called near-field light. In optics, in contrast to near-field light, the propagating light is then called far-field light. In order to utilize or detect the near-field light, a probe or detector needs to be introduced to the immediate vicinity of a sample. This method is firstly proposed by Synge in 1928 and experimentally realized by Pohl in 1984.[11] With its high spatial-resolving power, this method attracts a

lot of attentions and becomes a new research branch named near-field optics.[6, 11-15] It is worth to mention that the development of near-field optics is greatly supported and accelerated by SPM. Because SPM makes it possible to control a probe to go into the near-field region which is especially less than 100 nm[14, 15]. By combining of near-field optics and SPM, the method for optical imaging gets a new name as near-field scanning optical microscopy (NSOM). Today, NSOM has been well used in many fields to detect optical signals in nanometer scale.

Because near-field light is non-propagating, it cannot be detected by traditional optical system. In order to detect it, it needs to be transformed or converted to far-field light. Therefore, the detection of near-field light strongly depends on the light-matter interaction such as scattering and absorption. Technically, for near-field optical microscopy it detects tunneling photons in contrast to STM detects tunneling electrons.[16] Therefore, if we harness near-field light from samples, it is possible to detect nano-scale photon information and obtain a high-resolution optical nano-image.

In the nano scale, the interaction between light and matter is fundamentally weak as it occurs in small volume. For optical contrast imaging, certain light intensity is necessary for imaging. How to enhance the light intensity in the nanoscale volume? Thanks to the study of plasmonics,[8, 17-20] With the assistance of LSPR, enhanced light-matter interaction can be carried out and near-field information is probed by the same metal nanoparticle. This is a great idea for the near-field microscopy and spectroscopy. Recently, many high-resolution optical imaging techniques have been developed by utilizing this LSPR assisted detection, especially like tip-enhanced Raman microscopy and tip-enhanced fluorescence microscopy. They have shown their great power in application of imaging and characterization of nano-materials.

The ability of Raman spectroscopy to measure the frequencies of molecular and crystal vibrations has led to an extensive interest in the last decade in tip-enhanced Raman scattering (TERS). When local electric fields are resonantly excited at a metallic tip by laser irradiation under optimal condition, highly localized electric field enhancement can be produced. Such that if a nano-material is placed close to the tip, an enhancement factor of Raman scattering intensity of the order of 10^3 can be expected on

the sample surface beneath the tip over an area of diameter ~ 30 nm.[21, 22] In such high spatial resolution, TERS allows Raman imaging of single molecules. In addition to the application of TERS to the study of single-walled carbon nanotubes (SWNTs) by Hartschuh et. al.[23-25] and Yano et.al..[26, 27] TERS has now been applied successfully to a range of systems. TERS measurements by Pettinger et. al. of monolayers of absorbates on gold or platinum surfaces[28, 29] have demonstrated tip enhancement of Raman signal, with evidence of Raman scattering from single dye molecules.[29-31] Kawata group has shown how the strain induced through the application of mechanical pressure by the Ag-coated tip to adenine nanocrystals,[22, 32] C_{60}[33], and SWNTs[34, 35] can be observed from shifts in near-field Raman spectra obtained from TERS measurements and have employed TERS to study nanoscale strain in silicon surfaces.[36, 37] Biological applications of TERS have been demonstrated by Deckert et. al. who have measured Raman signals of DNA bases[38]. The progress for using TERS in liquid that is more universal in biology has been demonstrated by Zenobi et. al. recently.[39]

The enhanced electric field produced at a metallic tip under optimal laser irradiation can also be used to enhance fluorescence emission from molecules or quantum dots. Near-field fluorescent images of quantum dots,[40-42] single molecules,[43] and DNA[44] have all been observed. However a metallic tip in the vicinity of a fluorophore also leads to significant modifications to the radiative and nonradiative decay rates, as well as an enhancement in local incident field and, hence, excitation rate.[43, 45-51] The enhanced local field and radiative decay rate tend to increase the fluorescence intensity, while the increased nonradiative decay rate, which results from energy transfer from the fluorophore to metal, will diminish the fluorescence intensity dramatically. The net enhancement of fluorescence results from a competition between this enhancement and quenching. This leads a value of enhanced field or fluorescence resting at a certain value of tip-sample separation that can be considered as the optimized value. To have a high quality fluorescence image, the optimized tip-sample separation needs to be found.

1.4 Outline

In this study, I investigate the plasmonic enhancement and quenching in tip-enhanced fluorescence microscopy. The tip-sample separation dependent enhancement and quenching is successfully obtained, indicating an optimal tip-sample separation corresponding to the largest enhanced fluorescence intensity. Tip-enhanced fluorescence nano-imaging of quantum dots at this optimal tip-sample separation is achieved, demonstrating sub-wavelength resolution.

In the next Chapter, fluorescence, plasmonic enhancement, tip-enhanced Raman scattering, tip enhancement and quenching in fluorescence, and the requirement of optimization of tip-sample separation for tip-enhanced fluorescence are described.

In Chapter 3, a technique for controlling tip-sample separation is explained. This tip-sample separation control is achieved by utilizing a tapping-mode atomic force microscope (AFM). As a tip oscillates sinusoidally in tapping-mode AFM, tip-sample separation varies dynamically with oscillation time. A synchronization of tapping oscillation and photon detection is implemented. Hence, time-correlated photon counting can be obtained. Because of the sinusoidal correlation of time and tip-sample separation, tip-sample separation dependent fluorescence intensity can be converted from time-correlated fluorescence intensity.

Chapter 4 describes the application of tip-sample separation control to tip-enhanced Raman scattering (TERS). Tip-sample separation dependent enhanced Raman scattering intensity is successfully detected, which indicates the enhancement of light field produced at the tip apex. In addition, with the advantage of detecting far-field and near-field Raman signals in one data of tip-sample separation dependent Raman intensity, in situ far-field subtraction can be carried out. Thus TERS imaging without far-field signal is obtained and images of single-walled carbon nanotubes with a resolution of less than 12 nm are demonstrated.

In Chapter 5, quantum dot and its optical properties are described since it is used as the sample. And tip-enhanced fluorescence related to enhancement and quenching is

presented. With the same method of tip-sample separation control, tip-sample separation dependent fluorescence intensity is obtained, which distinctly indicates a competing result from tip enhancement and quenching. The optimized tip-sample separation for high-quality fluorescence imaging is obtained. In addition, nano images at the optimized tip-sample separation are obtained.

Finally, conclusions and outlook are presented in Chapter 6.

References

1. G. Binnig, H. Rohrer, C. Gerber and E. Weibel, Physical Review Letters **49** (1), 57-61 (1982).
2. G. Binnig, C. F. Quate and C. Gerber, Physical Review Letters **56** (9), 930-933 (1986).
3. L. Gross, Nature Chemistry **3** (4), 273-278 (2011).
4. P. Verma, T. Ichimura, T. Yano, Y. Saito and S. Kawata, Laser & Photonics Reviews **4** (4), 548-561 (2010).
5. Z. Anatoly and R. David, *Nano-Optics and Near-Field Optical Microscopy*. (Artech House, 2009).
6. S. Kawata, M. Ohtsu and M. Irie, *Near-Field Optics and Surface Plasmon Polaritons*. (Springer, 2001).
7. A. V. Zayats, I. I. Smolyaninov and A. A. Maradudin, Physics Reports **408** (3–4), 131-314 (2005).
8. S. Kawata, Y. Inouye and P. Verma, Nature Photonics **3** (7), 388-394 (2009).
9. E. Hutter and J. H. Fendler, Advanced Materials **16** (19), 1685-1706 (2004).
10. K. A. Willets and R. P. Van Duyne, Annual Review of Physical Chemistry **58** (1), 267-297 (2007).
11. D. W. Pohl, U. C. Fischer and U. T. Dürig, Journal of Microscopy **152** (3), 853-861 (1988).
12. E. Betzig and J. K. Trautman, Science **257** (5067), 189-195 (1992).
13. S. Kawata, Y. Inouye and T. Ichimura, Science Progress **87** (1), 25-49 (2004).
14. L. Novotny, Progress in Optics (2007).
15. D. W. Pohl, Philosophical Transactions of the Royal Society of London. Series A: Mathematical, Physical and Engineering Sciences **362** (1817), 701-717 (2004).
16. D. Courjon and C. Bainier, Reports on Progress in Physics **57** (10) (1994).
17. S. A. Maier, *Plasmonics: Fundamentals and Applications*. (Springer, 2007).
18. M. I. Stockman, Physics Today **64** (2), 39-44 (2011).
19. M. Pelton, J. Aizpurua and G. Bryant, Laser & Photonics Reviews **2** (3), 136-159 (2008).
20. W. L. Barnes, A. Dereux, and T. W. Ebbesen. Nature **424**, 824-830 (2003).

21. T.-a. Yano, T. Ichimura, A. Taguchi, N. Hayazawa, P. Verma, Y. Inouye and S. Kawata, Applied Physics Letters **91** (12) (2007).
22. H. Watanabe, Y. Ishida, N. Hayazawa, Y. Inouye and S. Kawata, Physical Review B **69** (15) (2004).
23. A. Hartschuh, E. J. Sánchez, X. S. Xie and L. Novotny, Physical Review Letters **90** (9) (2003).
24. A. Hartschuh, H. N. Pedrosa, J. Peterson, L. Huang, P. Anger, H. Qian, A. J. Meixner, M. Steiner, L. Novotny and T. D. Krauss, ChemPhysChem (2005).
25. A. Hartschuh, H. Qian, A. J. Meixner, N. Anderson and L. Novotny, Journal of Luminescence **119–120** (0), 204-208 (2006).
26. N. Hayazawa, T. Yano, H. Watanabe, Y. Inouye and S. Kawata, Chemical Physics Letters **376** (1-2), 174-180 (2003).
27. T. Yano, P. Verma, S. Kawata and Y. Inouye, Applied Physics Letters **88** (9) (2006).
28. B. Pettinger, B. Ren, G. Picardi, R. Schuster and G. Ertl, Physical Review Letters **92** (9) (2004).
29. K. F. Domke, D. Zhang and B. Pettinger, Journal of the American Chemical Society **128** (45), 14721-14727 (2006).
30. J. Steidtner and B. Pettinger, Physical Review Letters **100** (23) (2008).
31. B. Pettinger, Molecular Physics **108** (16), 2039-2059 (2010).
32. T. Ichimura, S. Fujii, P. Verma, T. Yano, Y. Inouye and S. Kawata, Physical Review Letters **102** (18) (2009).
33. P. Verma, K. Yamada, H. Watanabe, Y. Inouye and S. Kawata, Physical Review B **73** (4) (2006).
34. T.-a. Yano, Y. Inouye and S. Kawata, Nano Letters **6** (6), 1269-1273 (2006).
35. T.-a. Yano, P. Verma, Y. Saito, T. Ichimura and S. Kawata, Nature Photonics, 1-5 (2009).
36. Y. Saito, M. Motohashi, N. Hayazawa, M. Iyoki and S. Kawata, Applied Physics Letters **88** (14) (2006).
37. N. Hayazawa, M. Motohashi, Y. Saito, H. Ishitobi, A. Ono, T. Ichimura, P. Verma and S. Kawata, Journal of Raman Spectroscopy **38** (6), 684-696 (2007).

38. A. Rasmussen and V. Deckert, Journal of Raman Spectroscopy **37** (1-3), 311-317 (2006).
39. T. Schmid, B.-S. Yeo, G. Leong, J. Stadler and R. Zenobi, Journal of Raman Spectroscopy **40** (10), 1392-1399 (2009).
40. J. M. Gerton, L. A. Wade, G. A. Lessard, Z. Ma and S. R. Quake, Physical Review Letters **93** (18) (2004).
41. F. M. Huang, F. Festy and D. Richards, Applied Physics Letters **87** (18) (2005).
42. C. Xie, C. Mu, J. R. Cox and J. M. Gerton, Applied Physics Letters **89** (14) (2006).
43. P. Anger, P. Bharadwaj and L. Novotny, Physical Review Letters **96** (11) (2006).
44. Z. Ma, J. M. Gerton, L. A. Wade and S. R. Quake, Physical Review Letters **97** (26) (2006).
45. E. Dulkeith, A. C. Morteani, T. Niedereichholz, T. A. Klar, J. Feldmann, S. A. Levi, F. C. J. M. van Veggel, D. N. Reinhoudt, M. Möller and D. I. Gittins, Physical Review Letters **89** (20) (2002).
46. R. Carminati, J. J. Greffet, C. Henkel and J. M. Vigoureux, Optics Communications **261** (2), 368-375 (2006).
47. N. A. Issa and R. Guckenberger, Optics Express **15** (19), 12131-12144 (2007).
48. N. Hayazawa, K. Furusawa, A. Taguchi, S. Kawata and H. Abe, Applied Physics Letters **94** (19) (2009).
49. E. Yoskovitz, I. Hadar, A. Sitt, I. Lieberman and U. Banin, The Journal of Physical Chemistry C **115** (32), 15834-15844 (2011).
50. S. Kühn, U. Hakanson, L. Rogobete and V. Sandoghdar, Physical Review Letters **97** (1) (2006).
51. V. V. Protasenko, A. Gallagher, M. Labardi and D. J. Nesbitt, SPIE **5188**, 254-263 (2003).

Chapter 2.
Fluorescence and tip-induced enhancement and quenching

In tip-enhanced fluorescence, the enhancement effect is originated from a plasmonic resonant state excited at the apex of a metallic nanotip. However, enhancement of fluorescence induced by the metallic tip competes with quenching of fluorescence that is induced by the metallic tip as well. It is thus significant to know enhancement and quenching and their effects on fluorescence. In this chapter, the optical process and characteristics of fluorescence are described. The mechanism of plasmonic enhancement is explained. In addition, the utilization of plasmonic enhancement generated at a metallic nanotip to Raman scattering and fluorescence is presented and problem of tip quenching is explained. Finally, the optimization of enhancement and quenching in tip-enhanced fluorescence is proposed and explained.

2.1 Fluorescence

Fluorescence is the emission of light from a substance that has absorbed light or some other type of energy. In fact, this light emission (energy radiation) is from electrons relaxation from high electronic state to low ground state in the substance. In nature, a variety of molecules can be excited to the high electronic states and subsequently relax through fluorescence emission. They are known as fluorophores. Most of time, the emitted light has a longer wavelength, and therefore the lower energy, than the absorbed light. Fluorescence has many practical applications, including fluorescence

spectroscopy for highly sensitive molecular detection and fluorescence microscopy for cellular or molecular imaging.[1, 2]

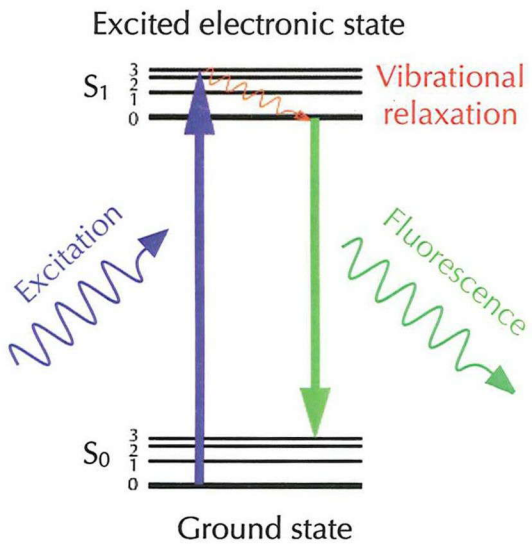

Figure 2.1.1 Jablonski diagram of fluorescence

The process of fluorescence is usually illustrated by the Jablonski diagram. Jablonski diagram is often used for discussing light absorption and emission, especially for the explanation of optical phenomena that can occur in excited states of electrons inside fluorophores. Figure 2.1.1 shows a typical Jablonski diagram. The ground, first excited electronic states are depicted by S_0 and S_1, respectively. S_1 contains more energy than S_0. Electrons at the ground and electronic states can exist in a number of sub-states, depicted by 0, 1, 2, etc. These sub-states are known as vibrational energy states originated from several different vibrational modes of the molecules. The transition from S_0 to S_1 depicted by a blue line means an absorption of excitation light. This process is estimated to happen in 10^{-15} second.[3] The following process depicted by a red wave is the non-radiative vibrational relaxation of electrons within time of about 10^{-12} second.[3] Vibrational relaxation ultimately leads energy to the form of heat. The green line in the graph indicates the final relaxation of electrons in a form of fluorescence. The time is in the order of 10^{-9} second.[3] Since vibrational relaxation is in 10^{-12} second much shorter than the time of fluorescence emission, so it is prior to

fluorescence emission. Hence fluorescence generally results from a thermally equilibrated excited state, that is, the lowest energy vibrational state of singlet excited electronic state. Also this is one of the reasons that fluorescence energy is usually lower than excitation energy. This results a shorter emitted wavelength than excitation wavelength. The difference of these wavelengths is known as the Stokes shift, which is the critical property that makes fluorescence so powerful. By completely filtering out the excitation light without blocking the emitted light, it is possible to see only the objects that are fluorescent. This is often utilized in fluorescence spectroscopy and microscopy. In an efficient optical detection system, this property could help to detect even a single molecule.[4]

Fluorescence is a radiative way of excited electrons to relax their excess energy. But the energy efficiency of fluorescence emission to absorption cannot reach to unity. Because unfortunately many other non-radiative pathways are available for the excited electrons to relax energy, such as intersystem crossing to a long living triplet state, energy transfer to the surrounding compounds, chemical reaction in the excited state and etc.. These pathways degenerate the fluorescence emission. In contrast to the radiative decay of fluorescence, they are considered as non-radiative decay processes. The total decay rate (γ_{tot}) consists of radiative decay rate (γ_r) and non-radiative decay rate (γ_{nr}). The ratio of radiative decay rate and the total decay rate is the quantum yields (η) denoted as equation (2-1). Many non-radiative decay channels are provided by the external environment. This makes fluorescence very environmental sensitive, which is also one of its important characteristics.[2] The great environment dependency of fluorescence makes it possible to search a way to achieve increased quantum yields and increased photostability.

$$\eta = \frac{\gamma_r}{\gamma_r + \gamma_{nr}} \qquad (2\text{-}1)$$

One of the interesting aspects of fluorescence is that one or several non-radiative decay channels compete with radiative emission, such as quenching process. Quenching decreases the intensity of fluorescence in a reversible way. It can occur by different mechanisms. For instance, collisional quenching occurs when the excited-state

fluorophore is deactivated upon contact with some other molecules in solution. Through collisions, due to different compounds of fluorescent sample and quenching objects, electron transfer or energy transfer could happen to release the excess energy of excited electrons. Fluorescence quenching in the vicinity of the metal surface has always been observed in many studies.[5-7] Because metals are efficient energy absorber at optical frequencies and the energy is ultimately dissipated to heat. Due to excitation energy transferred to the metal, fluorescence is easily diminished or quenched. Quenching happens at a very short distance, typically less than 10 nm.[5, 8]

Fluorescence is well used as an imaging contrast in microscopy. Not only for its advantage of separated emission wavelength from excitation wavelength facilitates imaging process, but also for the high sensitive power of revealing the localization and measurement of light-matter interaction, even detection of intracellular optical process or a single molecule. For every microscopy, to obtain high-resolution image is always the important and critical goal to get visualization of a single molecule. Ultimately, it should overcome the conventional diffraction limit and reach the scale of a molecule or an atom, in other word, nanometer scale. Recently developed tip-enhanced fluorescence technique has well overcome this problem to help realize the imaging resolution to the nanoscale level. It is based on near-field optics, which is unlike conventional far-field optics. In near-field optics, it deals with the optical processes in a scale of less than 100 nm that is much smaller than the diffraction limit (about 300 nm). By combing near-field optics and fluorescence, imaging resolution of 10 nm has been reported.[9] In these studies, a metallic tip is used to give great enhancement acting as a nanoscale light source. As nanoscale light source raster scanning over a sample, nanoscale high-resolution fluorescence imaging can be achieved. In tip-enhanced fluorescence microscopy, until now many studies have been focused on getting enhancement from metallic nanotip and tried to avoid quenching problem. For instance, tip-sample separation is often maintained at several nanometers by shear-force microscopy. But the maintained tip-sample separation is not accurate to be the optimized value resulting form enhancement and quenching. In this study, I develop a new experimental technique to deal with the quenching problem and optimize quenching and enhancement in tip-enhanced fluorescence.

2.2 Surface plasmon polaritons and plasmonic enhancement

Surface plasmons (SPs) are abundant electron oscillations that exist at the surface of a conductor, usually a metal. They were widely recognized in the field of surface science following the pioneering work of Ritchie in the 1950s.[10] When SPs are interacted with a light wave, coherent electron oscillations can be driven by the light field, resulting the hybridized excitation of a so-called surface plasmon polariton (SPP). This SPP is essentially electromagnetic waves that are trapped at the surface of a metal because of its interaction with the free electrons of the metal. Thus, unlike light that can propagate far away from the source, SPPs are evanescent waves that cannot propagate due to their strong association with the coherent oscillations of free electrons. A significant property of SPPs is that they are shorter in wavelength than the light. Because the spatial resolution of an optical system is dependent on wavelength ($d = 0.61\lambda/NA$, d: diffraction limit, λ: optical wavelength, NA: numerical aperture). Hence, SPPs can provide a significant reduction in effective wavelength of an imaging system and a corresponding light concentration beyond the diffraction limit. This could lead to a substantial improvement in spatial resolution of optical imaging.

As we known, the wavelength of light λ is inversely proportional to the angular frequency, ω, as $\lambda = 2\pi c/\omega = 2\pi/k_0$, where c is the speed of light, k_0 is the free-space light wavevector. Since SPPs are electromagnetic waves, their mathematical form can be obtained from solving Maxwell's equations and the associated boundary conditions. The solution yields a SPP dispersion relation, that is the frequency-dependent SPP wavevector, k_{spp} shown in equation (2-2).[11] $\xi_m(\omega)$ is angular frequency dependent permittivity of the metal and ξ_d is permittivity of the dielectric material (air or glass substrate etc.).

$$k_{spp} = k_0 \sqrt{\frac{\xi_d \xi_m(\omega)}{\xi_d + \xi_m(\omega)}} \qquad (2\text{-}2)$$

Figure 2.2.1 illustrates dispersion curves of light and a SPP. The dispersion of light shows a linear relationship between angular frequency (ω) and waveveckor (k_x) in x direction along the surface of a metal whereas the dispersion of a SPP shows a bending curve. At the same frequency (ω), the SPP shows a larger waveveckor k_{spp} than light (k_0). That means the wavelength of SPP ($\lambda_{spp} = 2\pi/k_{spp}$) is shorter than the wavelength of light and thus the speed of SPP ($\lambda_{spp} = 2\pi V_{spp}/\omega$) is slower. Since frequency of light and SPPs are same, thereby light can be used to excite SPPs. But the light line and the SPP curve never cross each other, which means that SPP can not be excited by the propagating light. In order to excite SPP, light with slow speed needs to be introduced to couple with SPP. One example of slow light is the evanescent light produced in total internal reflection.[10]

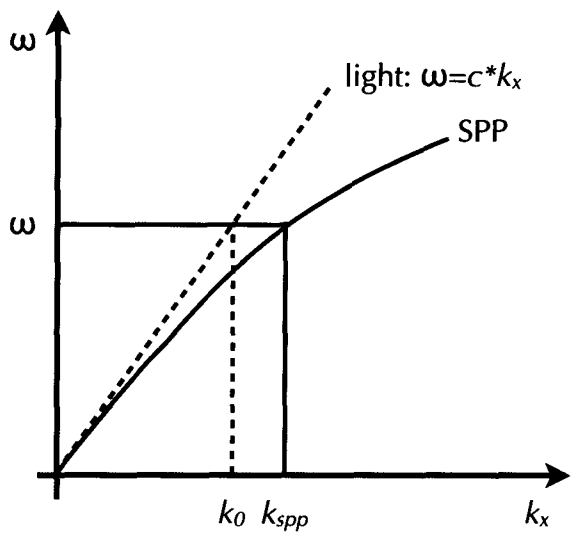

Figure 2.2.1 Dispersion curves of light and a SPP

The solution of SPP from Maxwell's equations also tells us the confinement of the electromagnetic field of SPP. Figure 2.2.2 illustrates the field distribution of a SPP in both sides of metal (ξ_m) and dielectric (ξ_d). The electric field of SPP (E_z) that is perpendicular to the metal-dielectric interface is enhanced near the interface and decaying exponentially with distance (Z) away from it. It is said to be evanescent, reflecting the bound or confined nature of SPPs, and preventing the field from propagating away from the interface. In the dielectric medium above the metal, the

decay length of the field, δ_d, is of the order of half the wavelength of light, whereas the decay length into the metal, δd, is determined by the penetration depth. Metals of silver and gold are the most commonly used materials to produce SPPs. Because the $\xi_m(\omega)$ of them is most suitable to provide a condition of small $\xi_m(\omega)+\xi_d$ to have a resonance in visible light. For instance, the penetration depth into silver of wavelength 630 nm on a silver-water interface is estimated to be 24 nm and for gold is 29 nm. And δ_d in the same situation is 219 nm for silver, and 162 nm for gold.[12]

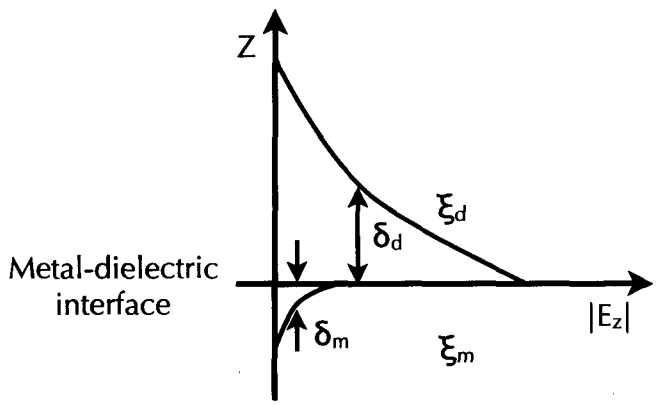

Figure 2.2.2 Field distribution of a SPP

Instead of a planar metal-dielectric interface, SPPs can also exist in other geometry, such as a metallic nanoparticle. In this case, the size of metallic nanoparticle is much smaller than the wavelength of light. The surface electromagnetic excitations on the surface of nanoparticles are called localized surface plasmons (LSPs). These LSPs are severely dependent on the shape and the size of the metallic nanoparticles. Because the size of nanoparticle is much smaller than wavelength, the electric field of an external excitation light can be approximated as a planar field to the nanoparticle, which allows us to solve Maxwell's equations using a quasi-static approximation. For a dipole oscillation mode of LSPs, a schematic excitation of LSPs is illustrated in Figure 2.2.3. Considering a metal particle in nanometer scale which is much smaller than light wavelength, when a light shines onto it, driven by the light field, the electrons of the metal particle can be periodically displaced with respect to the lattice metal ions. The displacement creates charges at opposite surfaces. Because those charges attract each other, there also exists an internal restoring force. The result is that electron oscillations

are created and so are the corresponding electromagnetic fields. The confinement of surface plasmons leads to an enhancement of electromagnetic fields. At a resonant oscillation of localized surface plasmons, electromagnetic field produced in the vicinity of a metal nanoparticle can be greatly enhanced.

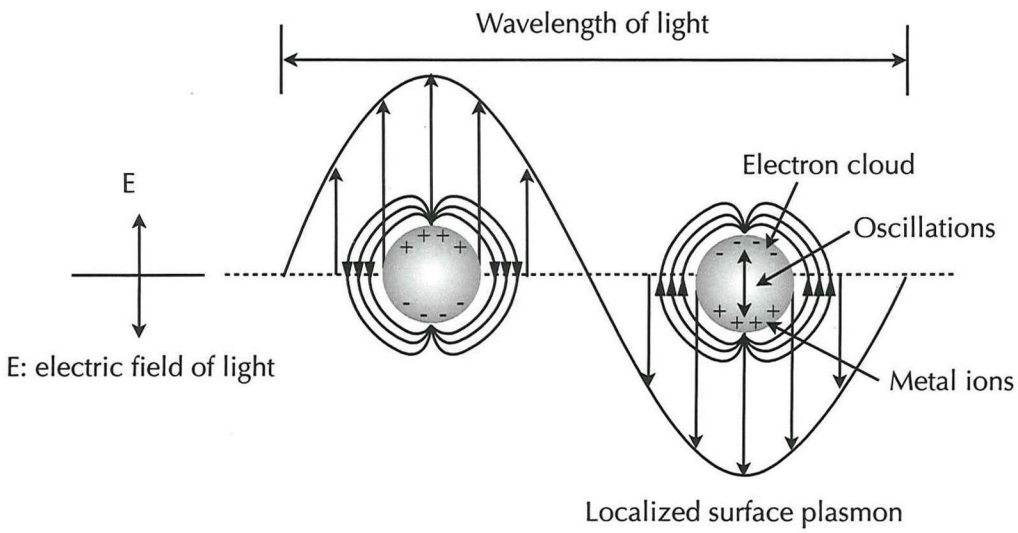

Figure 2.2.3 Schematic diagram of a localized surface plasmon

The resonance of LSPs is strongly dependent on the shape and size of a metallic nanoparticle.[13, 14] An easy way to understand the localized surface plasmon resonance is to consider the separation of free charge carriers under the influence of the external electric field of light. This separation creates an additional field that oscillates with the same frequency as the external field. As a result, an extremely localized and enhanced light field is created close to the metal structure.[15] As can be imaged that free charge carriers are more concentrated at curvature under oscillations, sharp corners of a metal nanostrucure can support strong resonances and hence supports stronger enhancement.[16] An interesting structure is nanocone or nanotip, which, owing to its sharp edge allowing to concentrate free charge carriers, can produce a strong field enhancement near the apex. The strong resonant oscillations and enhanced fields driven by light field at the metallic nanotip are illustrated in figure 2.2.4. Such a structure was proved to have a greatly localized field enhancement at the apex by Kawata group in 1998.[17] And it has

been used to enhance optical signals for high-sensitive spectral detection[18, 19] and high-resolution nano-imaging.[20, 21]

The enhanced field under a metallic nanotip is particularly dependent on the polarization of the incident light field. This is attributed to the localized mode of SPPs that has a tendency to oscillate along the tip axis. Theoretically and experimentally, it has been proved that p-polarization (parallel to tip axis) excitation light can produce much stronger field enhancement at the tip apex than s-polarization light (perpendicular to tip axis).[17, 22] Since localized mode of SPPs is strongly dependent on the dielectric constant of the metal and needs resonant wavelength excitation, it is important to choose the shape, size and material of different metals.[23, 24]

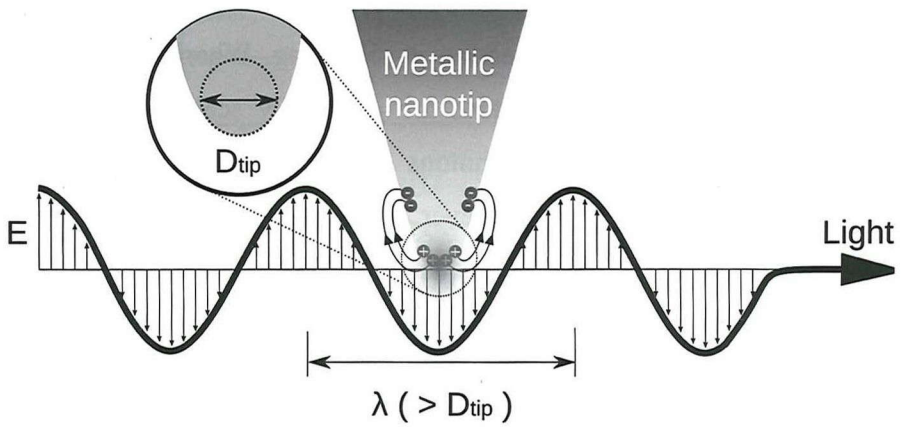

Figure 2.2.4 Light field enhancement at a metallic nanotip

Due to the unique confinement and enhancement of SPPs, especially the localized mode of SPPs (LSPs), they have been extremely well used in enhancing optical signals, such as Raman scattering and fluorescence. As described in the diffraction limit, to achieve high-resolution optical imaging, the effective short wavelength is required. Localized mode of SPPs possesses much shorter wavelength than propagating light. Additionally, they can be excited by a free-space propagating light in visible range. Therefore, They are particularly feasible for high-resolution optical imaging. Moreover, localized mode of SPPs provides enhanced light field sized about several tens of nanometers, which makes it possible to achieve optical sensing at a region far beyond diffraction limit. This also overcomes the problem of sensing samples with originally

weak optical signals from single molecules. To have a metallic nanotip scan over a sample, we can obtain enhanced optical intensity signals and construct a nano-image. Therefore, localized mode of SPPs generated at the apex of a metallic nanotip is essentially useful in near-field microscopy and spectroscopy. Recently, many high-resolution optical imaging techniques have been developed by utilizing this localized mode of SPPs assisted detection. Especially tip-enhanced Raman and fluorescence microscopy are developed by combining an optical microscope with a scanning probe microscope.

2.3 Tip-enhanced Raman scattering (TERS)

One of results from light-matter interaction is scattering. When photons are scattered from an atom or molecule, most photons are elastically scattered that is known as Rayleigh scattering. The scattered photons have the same kinetic energy and wavelength as the incident photons. However, a small fraction of the scattered photons are inelastically scattered that have a frequency different from the incident photons. This is known as Raman scattering that bears the name from its discoverer C. V. Raman.[25] Raman scattering corresponds to the absorption and subsequent emission of a photon via an intermediate quantum state of a substance. The intermediate quantum state can be either a real or a virtual energy state. There are two possible outcomes of Raman scattering. When the scattered photon has a lower energy than the incident photon, this outcome is labeled Stokes Raman scattering. In addition, when the scattered photon has a larger energy than the incident photon, the outcome is labeled anti-Stokes Raman scattering. The energy difference between scattered photon and incident photon corresponds to a resonant vibrational state of a substance and is independent of the energy of incident photon. Figure 2.3.1 illustrates Rayleigh scattering, Stokes Raman scattering and anti-Stokes Raman scattering according to the energy difference between incident photon and scattered photon. In fact, both Stokes and anti-Stokes Raman scattering can be excited at the same time, but Stokes Raman scattering is often stronger than anti-Stokes Raman. The intensity of Raman scattering depends on the population of the initial state of molecules. Because normally molecules initially tend to stay at the

ground state, thus Stokes Raman scattering is stronger than anti-Stokes Raman scattering at same excitation condition. Most commonly, the unit chosen in Raman spectrum is inverse centimeters (cm^{-1}), which express the Raman shift from the excitation wavelength.

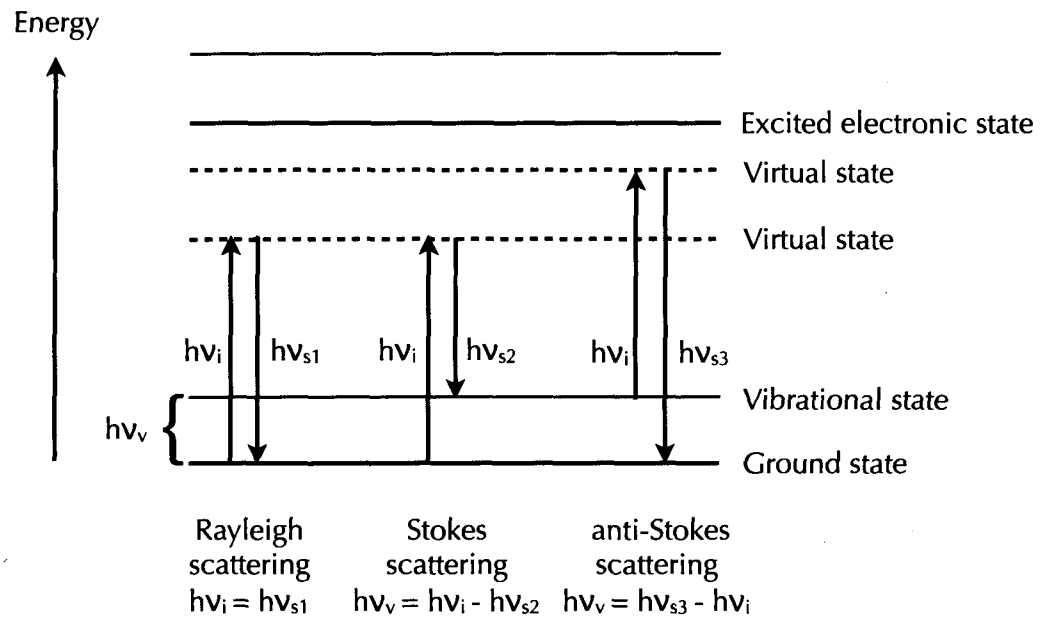

Figure 2.3.1 Different possibilities of light scattering

It is worth to mention that Raman scattering differs from the process of fluorescence. For fluorescence, the incident photon needs to be completely absorbed and the energy system inside a material goes to a real excited electronic state from which it can relax to ground state after a certain resonance lifetime. But for Raman scattering, the scattering process is as fast as absorption. There is no actual lifetime staying at the virtual state. The major difference is that Raman scattering can take place for any frequency of the incident light. In comparison with fluorescence that is a resonant effect of electronic states, Raman scattering is a resonant effect of vibrational states. In practice, a fluorescence peak is anchored at a specific frequency; a Raman peak maintains a constant separation from the excitation frequency.

One big problem of Raman scattering is that it is very weak. Typically it has extremely small cross section of ~10^{-30} cm^2. In contrast, fluorescence has a typical cross

section of ~10^{-16} cm^2. This problem can be dramatically improved by using plasmonic enhancement from metallic nanoparticles. By putting samples on a rough metallic surface, Raman scattering can been greatly enhanced by the enhanced field near metallic nanoparticles. This is now well known as surface enhanced Raman scattering (SERS). The nanoparticles with subwavelength dimension can be regarded as an accumulation of so called hot-spots where localized surface plasmon resonances can be excited and a strong electromagnetic field is generated. The enhancement factor of SERS is claimed by many researchers to be ~10^{15} that is suitable for single molecules detection.[26, 27] Derived from SERS, by considering to generate a sole enhanced field from only one metallic nanotip, tip-enhanced Raman scattering (TERS) has shown its power of high resolution Raman imaging. TERS overcomes the drawbacks of varying signal enhancements along the surface (due to its required roughness) and the lack of spatial resolution in SERS. The localized mode of SPPs explained in the second section of this chapter is the main reason for the enhancement in TERS. A TERS setup is realized by integrating an atomic force microscope (AFM) or scanning tunneling microscope (STM) (with a single metallic nanotip acting as a sole field enhancing site) with an optical microscopic system for Raman detection. By approaching a metallic nanotip controlled by AFM or STM close to the vicinity of a sample, Raman intensity can be greatly enhanced. Figure 2.3.2 shows a tip-enhanced Raman spectrum from single-walled carbon nanotubes (SWNTs) when an Ag-coated AFM tip is approached to be in contact with SWNTs. In contrast, a far-field Raman spectrum is also presented by retracting the nanotip away from the sample. Apparently, tip-enhanced Raman spectrum exhibits high intensity as 2 times stronger than far-field Raman spectrum at G Raman mode of SWNTs. It is a demonstration of the plasmonic enhancement effect induced from the metallic nanotip.

One important advantage of TERS is that the combination of Raman spectroscopy with scanning probe microscopy provides optical and topographic characterization in a single experiment. Altogether the optical and structural information can help analysis sample feasibly.

The spatial resolution of TERS is similar as AFM that is determined purely by the diameter of the metallic nanotip. To date, resolution of TERS imaging is reported to be

around 15 nm or smaller.[28, 29] This high resolution mainly originates from the plasmonic enhancement of the metallic nanotip. However, beyond this electromagnetic (EM) field interaction between tip and sample, chemical and mechanical interactions are investigated and proved to have more power to improve spatial resolution. The way to distinguish these interactions is to control tip-sample distance. With decreasing the tip-sample distance, EM interaction firstly occurs and then chemical interaction occurs if metal does electron transfer with the molecules. When the tip physically contacts or even deforms the sample, mechanical interaction occurs to shift Raman frequency. This mechanical interaction has been studied by Kawata group and proved that can be utilized to have a Raman image with a resolution as high as 4 nm.[30, 31]

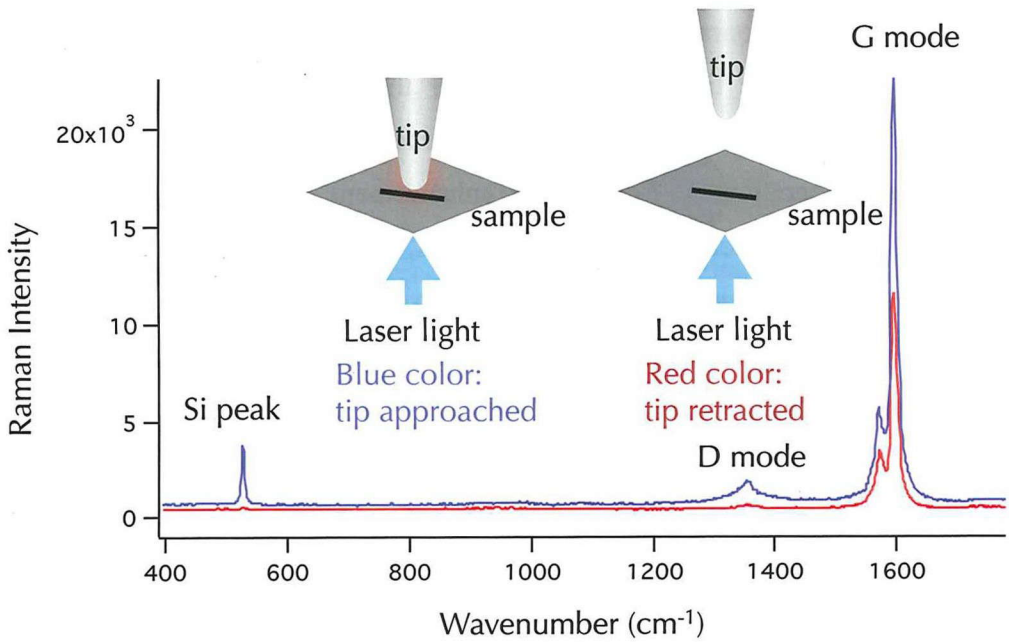

Figure 2.3.2 Illustration of tip-enhanced Raman spectrum from SWNTs

2.4 Tip-enhanced fluorescence

Fluorescence microscopy is particularly powerful for studying biological systems because of its sensitivity to single molecules. The major limitation is its diffraction limited resolution. Here, the signal enhancement provided by the metallic nanotip can

serve mainly to increase the spatial resolution due to the strongly confined enhanced light field. There are many examples of tip-enhanced fluorescence microscopy that use one- or two-photon excitation, exhibiting the great power of high-resolution nano-imaging.[9, 32-34] The enhanced field at the tip apex causes a local increase in the fluorescence-excitation rate, and the resulting emission is then detected to be larger than the normal fluorescence-excitation without the tip.

In a fluorescent system, the fluorescence depends on two factors, the external excitation rate (γ_{ex}) and the internal quantum yield (η). Thus fluorescence (S) can be written as $S \propto \gamma_{ex} . \eta$. The excitation rate depends both on the local field around the fluorophore and the field polarization. The quantum yield is determined by the radiative decay rate (γ_r) and nonradiative decay rate (γ_{nr}) as shown in equation 2-1. In the presence of a metallic tip, it may be smaller than the unperturbed quantum yield (absence of tip), in the case of fluorescence quenching, or larger than the unperturbed quantum yield where there is fluorescence enhancement. Theory studies predict that, in short metallic-nanoparticle-fluorophore distances, typically less than 5 nm, quenching dominates over enhancement.[35, 36] This is due to the short-range energy transfer from fluorophore to the metal surface. Therefore, if the tip-sample distance is larger than 5 nm or purposely controlled to be larger than 5 nm or by using semiconductor nanotip (e.g. Si) instead of metallic nanotip to avoid quenching, field enhancement from the nanotip can produce fluorescence enhancement dominating over quenching. This has been well observed in many studies about tip-enhanced fluorescence microscopy or spectroscopy.[9, 32, 37, 38]

2.5 Tip quenching in fluorescence

As we discussed in the first section, a fluorescent system can relax the excited energy not only through radiative decay process but also many possible non-radiative decay processes. For a metallic tip, for a distance between tip and a molecule, larger than 5 nm, radiative emission can be dominant, whereas for shorter distances the fluorophore will predominantly dissipate its excitation energy non-radiatively to the metal, thereby

quenching is dominant. This can be particularly proved in a nanoparticle-fluorophore system. When a metallic nanoparticle is chemically attached to a fluorophore, usually in molecular separation (much shorter than 5 nm), fluorescence quenching becomes very obvious.[5] Figure 2.5.1 is a schematic illustration of a nanoparticle-fluorophore system. In the left part, there is an unperturbed fluorescent system, by light excitation, fluorescence is emitted from a fluorophore. In the right part, a metallic nanoparticle is attached to the fluorophore. After the light excitation, because of the absence of band gap in metal, the excited energy can be easily transferred to the metallic nanoparticle and ultimately non-radiative dissipated to heat. Thus fluorescence is quenched. Such quenching phenomenon is often dominant at very short distances competing over the plasmonic enhancement. For a metallic nanotip, same quenching phenomenon happens at the short tip-sample distances.[39-43]

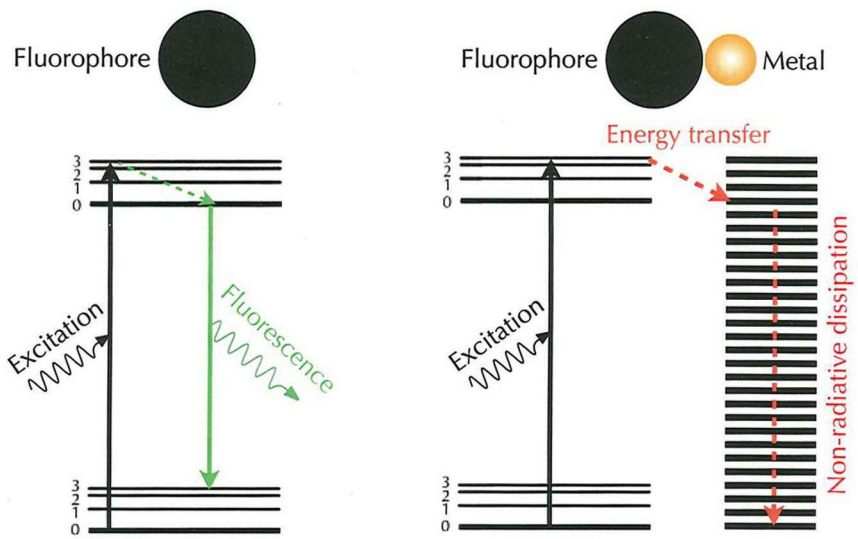

Figure 2.5.1 Fluorescence and quenching in a nanoparticle-fluorophore system

2.6 Optimization of tip-sample separation for tip-enhanced fluorescence

Till now we know that plasmonic enhancement effect can make a metallic tip to enhance optical signals. For Raman scattering, there is no quenching, therefore Raman

intensity has the same tendency of the enhanced field with respect to tip-sample distance. However, for fluorescence, with the advent of quenching, fluorescence intensity becomes different with respect to tip-sample distance. The difference is from the interaction between the metallic nanotip and the fluorophore. The effect of nearby metallic structures on fluorescence was studied theoretically and experimentally for spherical systems. Phenomenologically, what happens is the following: (1) If a dissipative structure (i.e., an extended piece of metal with free electrons and associated ohimic losses) is brought within the short range of near-field of a probe fluorophore, the near-field of the probe fluorophore induces motion of the electrons that quickly dissipate their gained energy (e.g., into heat). This opens up a new decay channel for the fluorophore-excited state with a nonradiative decay rate, γ_{nr} that allows deexcitation of the probe molecule without emission of a photon. For short distances, this nonradiative decay rate depends on the distance between the fluorophore and the extended metallic body as $1/r^3$, where r is the distance, reflecting the decay of the dipolar near field. It follows that for short distances, the rate k_{nr} dominates the radiate decay rate k_r and few photons are emitted by the probe molecule while the excited state lifetime decreases dramatically. This effect is usually called quenching. (2) If a suitable nanostructure (e.g., a metallic nanoparticle with a plasmon resonance, or a metal-coated tip) is brought in close proximity to the probe fluorophore within a proper separation between it and fluorophore, the spectrum of electromagnetic modes available for accepting a fluorescence photon from the probe fluorophore is changed. In the case of strong coupling to one or few modes of a resonant nano or microstructure, this leads to an enhanced emission of the coupled system with a likely strongly modified far-field emission pattern.

Figure 2.6.1 illustrates a schematic graph of fluorescence intensity as a function of tip-sample separation (D). From the view of plasmonic enhancement generated at the tip apex indicated by the blue line, fluorescence intensity should tend to be stronger as the fluorophore gets closer to the tip apex (shorter tip-sample separation). Plasmonic enhancement affects a near-field range of less than 20 nm. And then from the view of quenching indicated by the green line, fluorescence intensity should tend to be quenched or diminished as the fluorophore shortens its distance to the tip apex.

Quenching affects a near-field range of less than 5 nm. In total, plasmonic enhancement and quenching have the same source of metallic nanotip. These two effects can not be isolated and always compete with each other at the near-field tip-sample distances. Therefore, we can expect a combined result from effects of quenching and enhancement as indicated by the red line. Theoretically studies show that the largest fluorescence rests at a tip-sample separation of ~5 nm or less.

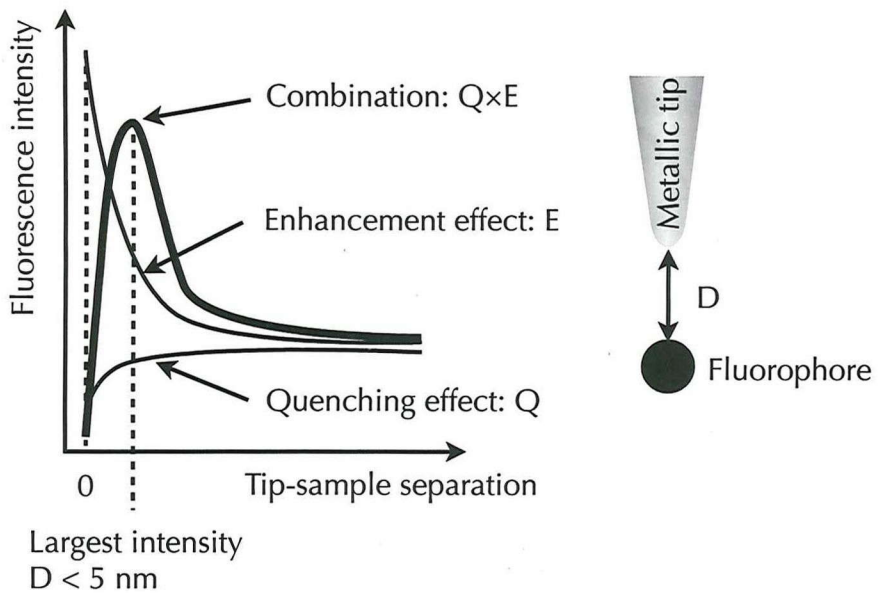

Figure 2.6.1 Schematic graph of fluorescence as a function of tip-sample separation

As a matter of fact, both enhancement and quenching are intensely tip-sample separation dependent. Therefore, to obtain the largest tip-enhanced fluorescence intensity, tip-sample distance control becomes a key part to be optimized. By using a sophisticated tapping-mode atomic force microscopy (AFM) system this distance control is realized easily in the near field. This concept is illustrated in figure 2.6.2. A tip can work in a periodical tapping way in tapping-mode AFM. This varies tip-sample separation periodically and the tip-sample separation can be exactly controlled in the near-field range. For a tapping oscillation loop, at the largest tip-sample separation indicated in the left graph of figure 2.6.2, we can detect far-field fluorescence excited by the laser; at a closer tip-sample separation indicated in the middle graph of figure 2.6.2, plasmonic enhancement is dominant and enhanced fluorescence is emitted; at the

minimum tip-sample separation indicated in the right graph of figure 2.6.2, quenching occurs to diminish fluorescence. With the help of tip-sample separation control in tapping-mode AFM, tip-sample separation dependent fluorescence can be obtained and the largest fluorescence intensity can be found at the optimized tip-sample separation. Then, with the technique of raster scanning, high-resolution and high contrast fluorescent imaging can be achieved at the optimized tip-sample separation.

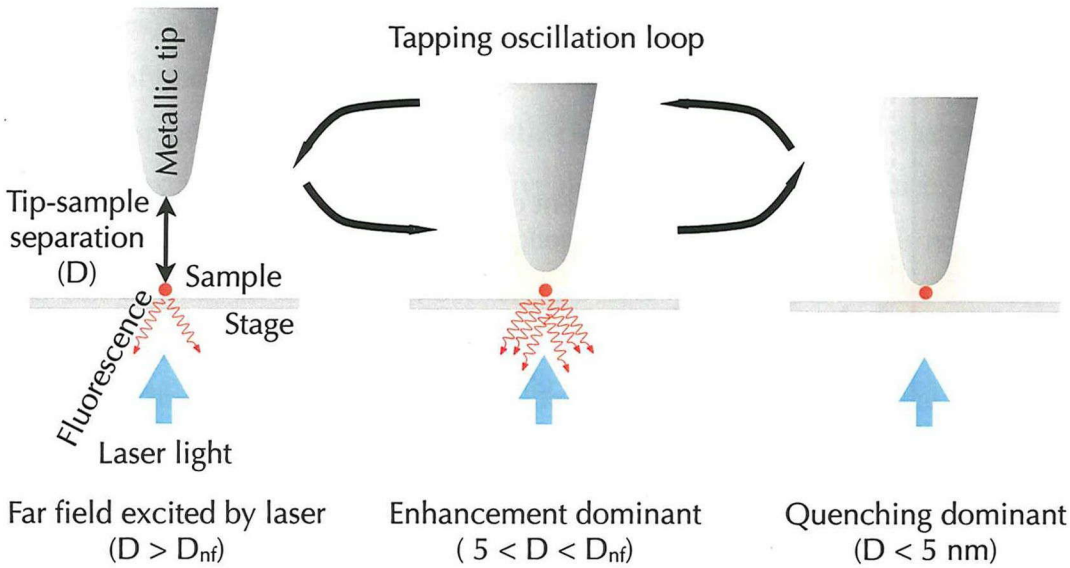

Figure 2.6.2 Tip-sample separation control for fluorescence intensity detection

References

1. B. Valeur and M. r. N. Berberan-Santos, Molecular Fluorescence. (John Wiley & Sons, 2012).
2. J. R. Lakowicz, Principles of Fluorescence Spectroscopy. (Springer, 2006).
3. J. W. Lichtman and J.-A. Conchello, Nature Methods 2 (12), 910-919 (2005).
4. X. S. Xie and R. C. Dunn, Science 265 (5170), 361-364 (1994).
5. E. Dulkeith, A. C. Morteani, T. Niedereichholz, T. A. Klar, J. Feldmann, S. A. Levi, F. C. J. M. van Veggel, D. N. Reinhoudt, M. Möller and D. I. Gittins, Physical Review Letters 89 (20) (2002).
6. B. Nikoobakht, C. Burda, M. Braun, M. Hun and M. A. El-Sayed, Photochemistry and Photobiology 75 (6), 591-597 (2002).
7. F. Cannone, G. Chirico, A. R. Bizzarri and S. Cannistraro, The Journal of Physical Chemistry B 110 (33), 16491-16498 (2006).
8. J. Azoulay, A. Débarre, A. Richard and P. Tchénio, EPL (Europhysics Letters) 51 (4) (2000).
9. J. M. Gerton, L. A. Wade, G. A. Lessard, Z. Ma and S. R. Quake, Physical Review Letters 93 (18) (2004).
10. W. L. Barnes and A. Dereux, Nature (2003).
11. S. A. Maier, Plasmonics: Fundamentals and Applications. (Springer, 2007).
12. J. Homola and S. S. Yee, Sensors and Actuators B: Chemical (1999).
13. A. J. Haes and R. P. Van Duyne, Journal of the American Chemical Society 124 (35), 10596-10604 (2002).
14. K. A. Willets and R. P. Van Duyne, Annual Review of Physical Chemistry 58 (1), 267-297 (2007).
15. S. Kawata, Y. Inouye and P. Verma, Nature Photonics 3 (7), 388-394 (2009).
16. J. T. Krug, E. J. Sanchez and X. S. Xie, The Journal of Chemical Physics 116 (24), 10895-10901 (2002).
17. H. Furukawa and S. Kawata, Optics Communications 148 (4-6), 221-224 (1998).
18. N. Hayazawa, Y. Inouye, Z. Sekkat and S. Kawata, Optics Communications 183 (1-4), 333-336 (2000).

19. N. Hayazawa, Y. Inouye, Z. Sekkat and S. Kawata, Chemical Physics Letters 335 (5-6), 369-374 (2001).
20. N. Hayazawa, Y. Inouye, Z. Sekkat and S. Kawata, The Journal of Chemical Physics 117 (3), 1296-1301 (2002).
21. T. Ichimura, N. Hayazawa, M. Hashimoto, Y. Inouye and S. Kawata, Physical Review Letters 92 (22) (2004).
22. L. Novotny, R. X. Bian and X. S. Xie, Physical Review Letters 79 (4), 645-648 (1997).
23. X. Cui, W. Zhang, B.-S. Yeo, R. Zenobi, C. Hafner and D. Erni, Optics Express 15 (13), 8309-8316 (2007).
24. A. Taguchi, N. Hayazawa, Y. Saito, H. Ishitobi, A. Tarun and S. Kawata, Optics Express 17 (8), 6509-6518 (2009).
25. R. Singh, Physics in Perspective (PIP) 4 (4), 399-420 (2002).
26. K. Kneipp, Y. Wang, H. Kneipp, L. T. Perelman, I. Itzkan, R. R. Dasari and M. S. Feld, Physical Review Letters 78 (9), 1667-1670 (1997).
27. S. Nie and S. R. Emory, Science 275 (5303), 1102-1106 (1997).
28. L. G. Cançado, A. Hartschuh and L. Novotny, Journal of Raman Spectroscopy 40 (10), 1420-1426 (2009).
29. J. Steidtner and B. Pettinger, Physical Review Letters 100 (23) (2008).
30. T. Ichimura, S. Fujii, P. Verma, T. Yano, Y. Inouye and S. Kawata, Physical Review Letters 102 (18) (2009).
31. T.-a. Yano, P. Verma, Y. Saito, T. Ichimura and S. Kawata, Nature Photonics, 1-5 (2009).
32. E. J. Sánchez, L. Novotny and X. S. Xie, Physical Review Letters 82 (20), 4014-4017 (1999).
33. N. Hayazawa, K. Furusawa, A. Taguchi, S. Kawata and H. Abe, Applied Physics Letters 94 (19) (2009).
34. H. G. Frey, S. Witt, K. Felderer and R. Guckenberger, Physical Review Letters 93 (20) (2004).
35. J. Azoulay, A. Débarre, A. Richard and P. Tchénio, Journal of Microscopy 194 (2-3), 486-490 (1999).

36. R. Carminati, J. J. Greffet, C. Henkel and J. M. Vigoureux, Optics Communications 261 (2), 368-375 (2006).
37. H. F. Hamann, A. Gallagher and D. J. Nesbitt, Applied Physics Letters 76 (14), 1953-1955 (2000).
38. A. Hartschuh, Philosophical Transactions of the Royal Society of London. Series A: Mathematical, Physical and Engineering Sciences 362 (1817), 807-819 (2004).
39. Y. Ebenstein, E. Yoskovitz, R. Costi, A. Aharoni and U. Banin, The Journal of Physical Chemistry A 110 (27), 8297-8303 (2006).
40. W. Trabesinger, A. Kramer, M. Kreiter, B. Hecht and U. P. Wild, Applied Physics Letters 81 (11), 2118-2120 (2002).
41. E. Yoskovitz, G. Menagen, A. Sitt, E. Lachman and U. Banin, Nano Letters 10 (8), 3068-3072 (2010).
42. P. Anger, P. Bharadwaj and L. Novotny, Physical Review Letters 96 (11) (2006).
43. S. Kühn, U. Hakanson, L. Rogobete and V. Sandoghdar, Physical Review Letters 97 (1) (2006).

Chapter 3.
Experimental technique for controlling tip-sample separation

As explained in the last chapter, the competition of plasmonic enhancement and quenching results an optimized tip-sample separation for tip-enhanced fluorescence microscopy. Therefore, determination of this optimized tip-sample separation is significant. Benefiting from dynamic control of tip-sample separation, atomic force microscopy working in tapping operation gives a feasible solution to measure the optimized tip-sample separation. In detail, the experimental technique for controlling tip-sample separation is described in this chapter.

3.1 Tapping operation of atomic force microscope

Atomic force microscopy (AFM) is a technique to characterize surfaces of a specimen at an extremely high spatial resolution, typically in nanometer scale.[1] Mechanistically, AFM operates based on the interaction forces between a nanotip and the specimen. The interaction forces totally can be regarded as repulsive forces or attractive forces at different tip-specimen distance. Repulsive forces dominate at shorter tip-specimen distance than attractive forces, especially when tip contacts with specimen. AFM can operate at different modes by measuring repulsive or attractive forces. In practice, AFM images are constructed with height information by scanning the nanotip or sample stage in a raster pattern. An active feedback loop is required to deal with the variation of interaction forces that is caused by roughness of specimen surface during scanning. In

the feedback loop, mostly a constant force is maintained. Usually maintaining a constant repulsive force results tip being in contact with the specimen. Thus AFM utilizing this method is known as contact mode AFM. In addition, non-contact of tip and specimen can be realized by measuring the attractive forces, which results non-contact mode AFM. In non-contact mode, the cantilever is oscillated at a frequency slightly above its resonant frequency where the amplitude of oscillation is typically a few nanometers (<10 nm).[2] In these a few nanometers attractive forces act to influence the oscillation. And a feedback loop restores the oscillation with a constant amplitude or frequency. Another operating mode of AFM is known as tapping mode. The cantilever is oscillated in tapping mode as well but with a larger oscillation amplitude (100~200 nm). The tip does intermittent contact with the specimen in the tapping oscillation. A feedback loop is utilized to maintain preset oscillation amplitude.

Contact mode AFM maintains cantilever (with a tip at its end) deflection as relevance of repulsive forces through the feedback system. In practice, a optical lever is used to monitor the deflection of cantilever. Laser light is usually incident to the top surface of the cantilever (opposite side to the tip). It is then reflected to a position sensitive photodetector (PSP) that collects the laser light. When the cantilever is deflected due to repulsive forces between tip and specimen, the produced displacement of light is detected by PSP and sent to the feedback system. In contact mode, tip is always in contact with the surface, which makes it easy to damage samples especially for soft ones.[3]

Non-contact mode AFM is preferable to contact mode AFM for measuring soft samples. However, the < 10 nm oscillation amplitude has some limitations. In ambient conditions, most samples develop a liquid meniscus layer[3]. This could make the tip stick to the sample surface.

By making the tip intermittent contact with the surface, tapping mode AFM becomes more useful for measuring soft samples and it can also prevent the tip from sticking to the surface. The tip is oscillated up and down at a frequency near its resonant frequency and an amplitude (100~200 nm) far beyond the region of attractive forces (< 10 nm). In such a way of tapping oscillation, the sample cannot be damaged as easily as

the sample in the contact mode AFM. Figure 3.1.1 illustrates a typical tapping mode AFM system. A cantilever oscillates periodically driven by an electric sinusoidal signal. When tip is approached to the sample surface, the oscillation amplitude is decreased due to the interaction forces.[4-6] The change of oscillation amplitude is monitored by the difference signal (DIF) of laser light that is collected by a position sensitive photodetector. A feedback control system monitoring Z direction is utilized to maintain the height of cantilever to restore the preset oscillation amplitude. Piezos are used to control Z direction displacement and X, Y direction raster scanning.

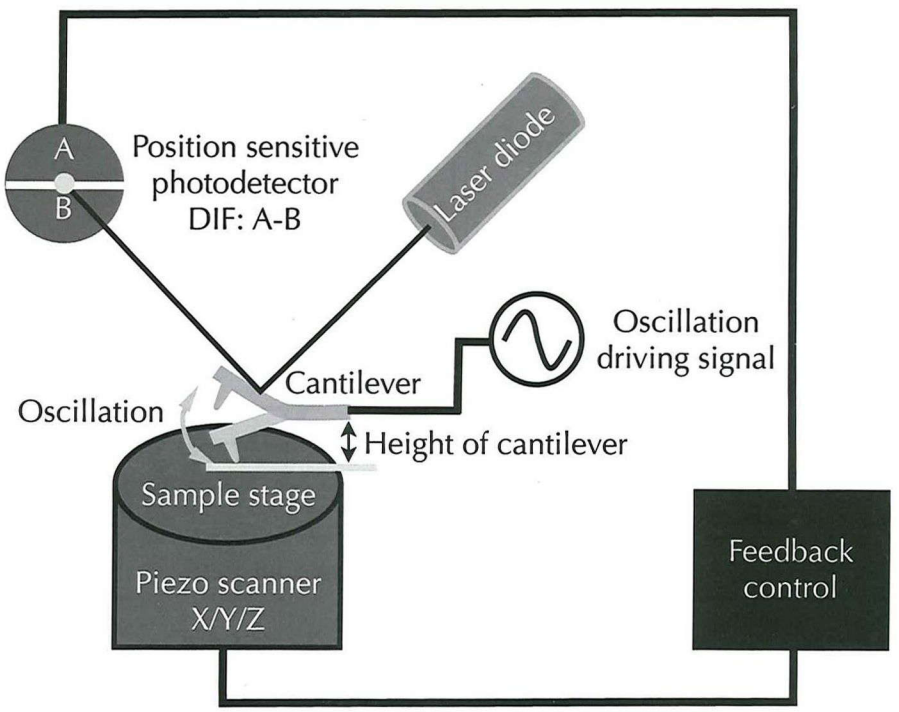

Figure 3.1.1 Tapping mode AFM system

For the purpose of studying the plasmonic enhancement and quenching in tip-enhanced fluorescence, our experimental setup is designed by utilizing a tapping mode AFM. As explained in Chapter 2, optimization of tip-sample separation is important for tip-enhanced fluorescence microscopy. Tapping mode AFM provides dynamic tip-sample separations, which make it possible to find out the optimal tip-sample separation for fluorescence imaging if we precisely detect the fluorescence with respect to its corresponding tip-sample separation. The periodical tapping oscillation facilitates the

implementation of our purpose. By synchronization of tapping oscillation (variation of tip-sample separation) with time-gated photon detection (fluorescence signal), the tip-sample separation dependency of fluorescence intensity is obtainable. In Chapter 2, the evanescent property of the enhanced field at the apex of a metallic nanotip is described. When the distance between tip and sample goes far enough, far-field signal can be separated. The evanescent field (E_{spp}) is illustrated in figure 3.1.2. In the direction of Z, the field strength decreases exponentially from near-field distance to far-field distance. In the study, we control the amplitude of oscillation to be ~100 nm. It is found that a constant intensity level of far-field signal can be measured in this range. Therefore, in situ far-field signal removal is feasible to get pure near-field signal.

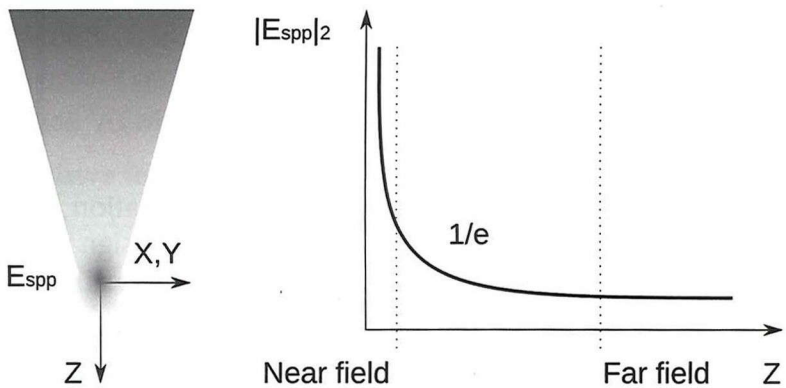

Figure 3.1.2 Near field and far field

Recently, some near-field optical microscopy combines a shear-force microscope (SFM) working in constant-height mode to locate at a very short tip-sample distance (~ 2 nm).[7, 8] SFM maintains lateral interaction forces parallel to the sample surface by a feedback system controlling lateral oscillation of the tip. The lateral force is known as shear force. SFM has the ability to hold a tip just a few nanometers above the surface of the sample. Although the constant height mode of SFM detects the very high localized near field, it is subject to misinterpretations because of the varying distance between tip and sample when scanning over structured surfaces, and the optical signal is far-field background included. For fluorescence imaging, this mode can additionally meet a problem disturbed by quenching. Such problems can be solved in tapping-mode AFM. Because tapping mode AFM has an advantage of detecting the variation of optical

signal from near field to far field, and eventually construct a far-field free optical image by simply far-field signal subtraction.

3.2 Dynamic tip-sample separation

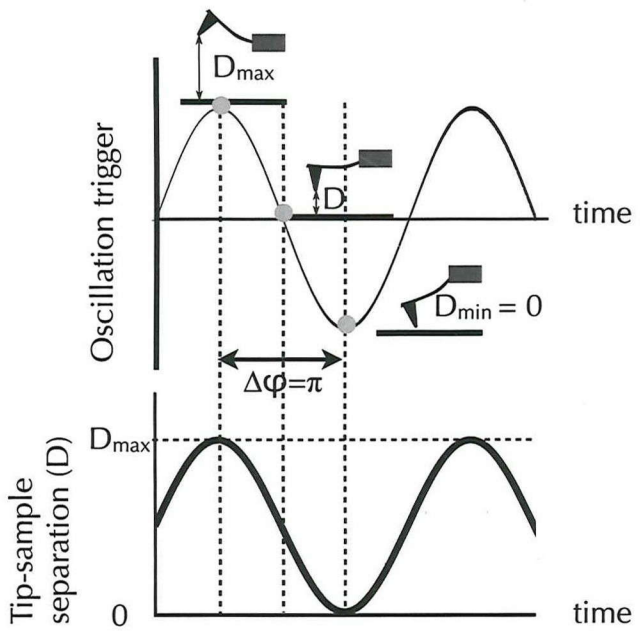

Figure 3.2.1 Tip-sample separation as a function of time

In our tapping-mode AFM, the cantilever is driven to oscillate up and down at a frequency a bit smaller than the resonance frequency by a sinusoidal electric signal. The amplitude of this oscillation is preset to be ~100 nm. In this nanoscale range, tip-sample separation dynamically changes as a function of time. Figure 3.2.1 illustrates the relation between tapping oscillation and tip-sample separation. The oscillation trigger is a sinusoidal wave shown in the top graph. At different phase of trigger oscillation, tip-sample separation has a certain value corresponding to it. Apparently, the maximum tip-sample distance and the minimum tip-sample distance has a phase difference of π. As the oscillation of the cantilever is driven by the sinusoidal signal, tip-sample separation is a sinusoidal function of time shown in the bottom graph. It can be denoted

as equation (3-1), where D is tip-sample separation, A is the oscillation amplitude and f is the oscillation frequency. This function helps us to know how to calculate tip-sample separation according to different time.

$$D = 2A \cdot (1 + \cos(2\pi \cdot f \cdot t)) \tag{3-1}$$

3.3 Time-correlated tip-sample separation

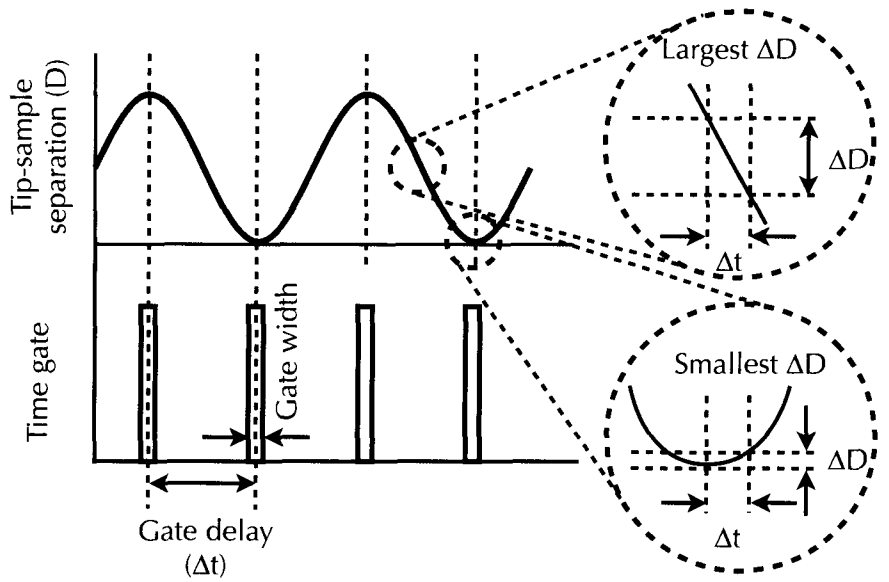

Figure 3.3.1 Schematic illustration of time gating for sectioning tip-sample separation

Since we know that tip-sample separation oscillates sinusoidally in tapping mode AFM, it is possible to divide tip-sample separation into many small sections by time gated method. In the time-gated method, gate delay determines the resolving power of tip-sample separation. Figure 3.3.1 shows a schematic illustration of time gating for sectioning tip-sample separation. As the gate width is small enough comparing to the oscillation period, it can be considered to correspond to a tip-sample separation. Thus the number of tip-sample separations can be calculated as a result from period divided by gate delay (Δt) in one oscillation period. Because tip-sample separation is a sinusoidal function of time, the interval of tip-sample separations is so very different at

the same gate delay. At the minimum tip-sample separation, the section (ΔD) of tip-sample separation is the smallest. In fact, in our experiment, it can reach to sub-nanometer scale with a fairly small gate delay. The same situation occurs at the maximum tip-sample separation as this position has the same sharpness of the sinusoidal curve. In contrast to this highest resolving power of tip-sample separation, the lowest section (ΔD) of tip-sample separation sits at the middle point between the maximum and the minimum tip-sample separation. Both situations with the same gate delay are enlarged in figure 3.3.1. Overall, the time-correlated tip-sample separation can be obtained by determining the gate delay.

3.4 Maximum tip-sample separation from force curve measurement

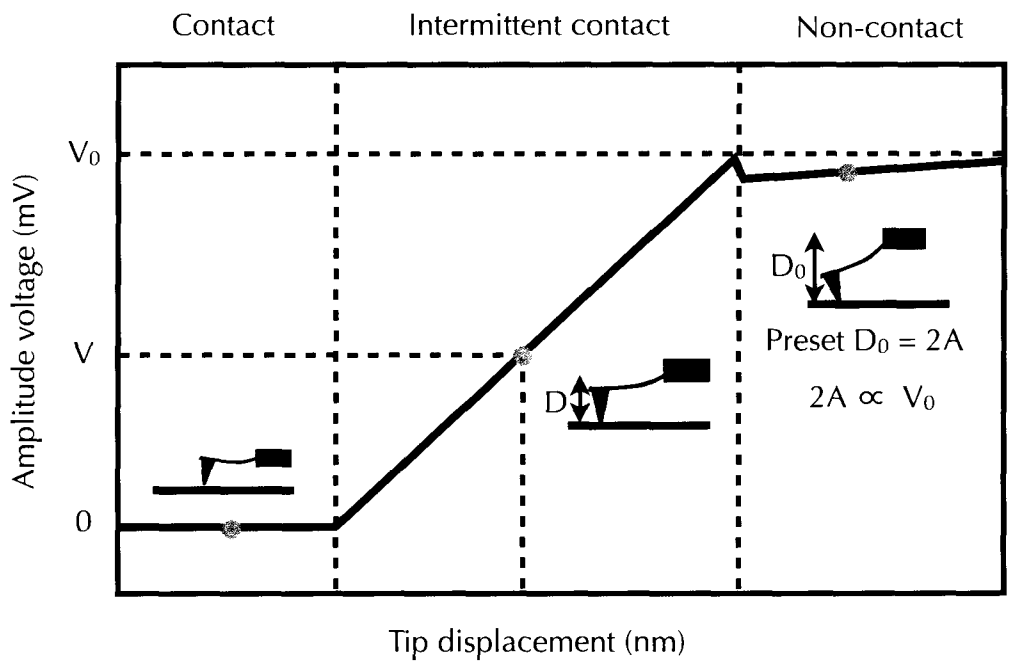

Figure 3.4.1 Process of force curve measurement

In tapping-mode AFM, constant oscillation amplitude is maintained by adjusting the height of the cantilever through piezoelectric voltage control. It is proportional to the amplitude voltage. The preset oscillation amplitude can be calculated by force curve

measurement.[9] In force curve measurement, the tapping tip is gradually approached to the sample surface from non-contact region to contact region without feedback control. Thus the oscillation amplitude gradually decreases as the interaction forces between tip and sample affect it in the intermittent contact region. The decrease of amplitude means the decrease of the amplitude voltage. Till the tip contacts with the sample, tip displacement gradually varies. This is shown in figure 3.4.1. The maximum tip-sample separation can be obtained from tip displacement as a function of amplitude voltage.

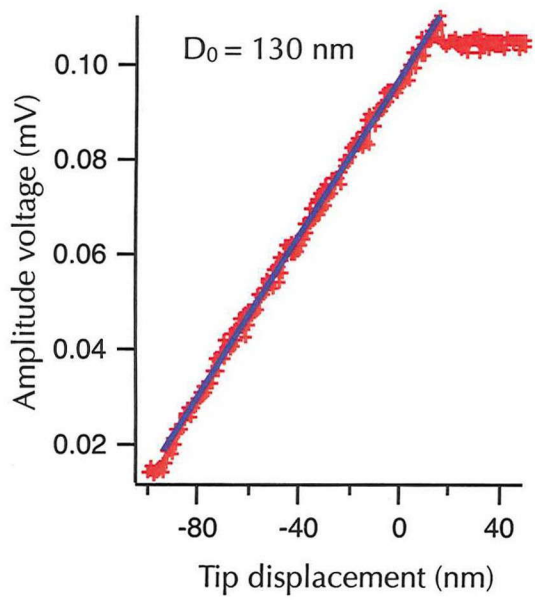

Figure 3.4.2 Experimental data of force curve measurement

In practice, because tip or sample has a high possibility to be damaged in contact region, we choose to measure part of the force curve to avoid any damages. It can be done by selecting the range of amplitude voltage in force curve measurement. For a instance, figure 3.4.2 shows an experimental force curve data. The red curve is the raw data indicating a relation between amplitude voltage and tip displacement. The blue line is a linearly fitted result from the red curve. Through a calculation of the tip displacement at amplitude voltage of 0 mV by the slope of the fitted line, the maximum tip-sample separation can be obtained from the total tip displacement in the intermittent contact region. It is found to be 130 nm in this experimental data.

3.5 Time to tip-sample separation conversion

As mentioned in section 3.2, tip-sample separation is a function of time, denoted as equation (3-1). The oscillation amplitude is half of maximum tip-sample separation ($D_0 = 2A$), that can be obtained from force curve measurement. The oscillation frequency (f) is determined by resonance frequency of the cantilever. It is usually smaller than the resonance frequency in our experiments. And in practice, it needs to be determined in Q curve measurement as one procedure in tapping mode AFM operation. Thus it is known as an initial value as well. Therefore, tip-sample separations can be obtained from equation (3-1) according to the delay time (t).

References

1. G. Binnig, C. F. Quate and C. Gerber, Physical Review Letters 56 (9), 930-933 (1986).
2. Y. Martin, C. C. Williams and H. K. Wickramasinghe, Journal of Applied Physics 61 (10), 4723-4729 (1987).
3. Q. Zhong, D. Inniss, K. Kjoller and V. B. Elings, Surface Science Letters 290 (1–2), L688-L692 (1993).
4. P. K. Hansma, J. P. Cleveland, M. Radmacher, D. A. Walters, P. E. Hillner, M. Bezanilla, M. Fritz, D. Vie, H. G. Hansma, C. B. Prater, J. Massie, L. Fukunaga, J. Gurley and V. Elings, Applied Physics Letters 64 (13), 1738-1740 (1994).
5. C. A. J. Putman, K. O. Van der Werf, B. G. De Grooth, N. F. Van Hulst and J. Greve, Applied Physics Letters 64 (18), 2454-2456 (1994).
6. I. Schmitz, M. Schreiner, G. Friedbacher and M. Grasserbauer, Analytical Chemistry 69 (6), 1012-1018 (1997).
7. E. J. Sánchez, L. Novotny and X. S. Xie, Physical Review Letters 82 (20), 4014-4017 (1999).
8. A. Hartschuh, H. Qian, A. J. Meixner, N. Anderson and L. Novotny, Journal of Luminescence 119–120 (0), 204-208 (2006).
9. T.-a. Yano, T. Ichimura, A. Taguchi, N. Hayazawa, P. Verma, Y. Inouye and S. Kawata, Applied Physics Letters 91 (12) (2007).

Chapter 4.

Application of tip-sample separation control to TERS

Tapping operation of atomic force microscopy demonstrates its feasibility for controlling tip-sample separation as a function of time. With synchronization of tapping oscillation and time-gated photon detection, it is possible to obtain optical signal (from the sample under the tapping tip) as a function of tip-sample separation. It is experimentally found that the tapping distance between tip and sample is an available range to get a far-field free optical signal in situ. As the tip-sample separation dependency of optical strength shows a separated far-field signal that can be subtracted afterward from the signal in the near-field region. The application of this experimental technique to tip-enhanced Raman scattering (TERS) is described in this chapter. Far-field free TERS imaging of SWNTs is achieved.

4.1 Tapping-mode TERS

In the last decade, TERS has become more and more useful and attractive as a method for Raman spectroscopy with high sensitivity[1-6] and nanoscale imaging with high spatial resolution.[7-12] These high sensitive and resolving powers relies on the plasmonic enhancement and spatial confinement of electromagnetic field at the apex of a metallic nanotip, which is explained in Chapter 2. The plasmonic enhancement is originated from the resonant coupling of external light field and surface plasmons at the metallic surface.[13-18] The confined and enhanced light field at the tip apex is evanescent, it cannot propagate away from the surface. This property ideally provides a tiny light

source with a size determined by the diameter of the tip apex. Typically the diameter at the apex of a metallic tip is 30-50 nm. If a sample is brought into the confined light field, Raman signal can be greatly enhanced due to the strong excitation from the enhanced field. This is often known as near-field Raman signal. As a result of the evanescent property of the enhanced light field, the strength of near-field Raman signal is strongly dependent on the separation between the tip and the sample. When the tip-sample separation increases, the enhanced field rapidly decreases causing the strength of near-field Raman signal to decrease as well. When the tip-sample separation is large enough to go out of the near-field range, Raman signal is only excited by the external light field that is usually a propagating light used to couple with surface plasmons. This Raman signal is known as far-field Raman signal. Unfortunately, since an external light field is initially required to generate a plasmonic light source, far-field Raman signal always comes along with near-field Raman signal at the confined near-field region. In conventional TERS microscopy, a scanning probe typed microscope such as shear force microscope (SFM)[19, 20] or contact-mode AFM[21] are usually integrated with an optical microscope. The tip is oscillated in the direction parallel to the sample surface in SFM, which can keep tip-sample distance constant (a few nanometers) in Z direction (along the tip axis) or the tip contacts with the sample in contact-mode AFM. In both cases, near-field Raman image constructed from Raman intensity obtained by raster scanning a metallic nanotip over the sample is always taken including the far-field Raman signal.[22-24] Or near-field and far-field Raman images are taken separately for the subtraction afterwards to get a pure near-field Raman image.[25] In the first case, the image contrast can be influenced if the enhancement is relatively weak while in the later case the twice-imaging processes are really time consuming.

In 2007, our group published a paper that introduced tapping-mode tip-enhanced Raman microscopy.[26] It utilized the tip-sample distance regulation in tapping-mode AFM[27, 28] to investigate the confinement of enhanced field. The method has an advantage of removing far-field Raman signal efficiently in a one-time raster-scanning process. A metallic nanotip is driven to oscillate in the direction perpendicular to the sample surface, which means tip-sample distance varies with time. As we mentioned that near-field Raman signal is tip-sample distance dependent. Therefore, if the tip-

sample distance variation in tapping-mode AFM can be controlled for Raman detection at different distances, it is able to detect the distance dependent Raman intensity and distinguish near-field Raman signal from far-field Raman signal in one measurement. In our system, we synchronize Raman detection system with the tapping oscillation of AFM. At each tapping position, Raman intensity is detected with respect to the specific tip-sample distance in one measurement. This synchronization helps to detect distance dependent Raman intensity that is efficient to not only evaluate the confinement of enhanced field but also subtract far-field signal in situ for imaging. As I introduced in Chapter 3, tapping-mode AFM can dynamically change tip-sample distance. It is found that the transition of Raman intensity from enhanced near-field signal (superimposed with far-field signal) to separated far-field signal can be observed in a range of ~100 nm tip-sample separation,. Thus a far-field free Raman image can be obtained by simply subtraction of far-field Raman intensity.

4.2 Experimental setup

Our experimental setup is based on an inverted oil-immersion optical microscope integrated with a tapping-mode AFM illustrated in figure 4.2.1(a). The sample stage is controlled by piezos and can be raster scanned to obtain an image. A continuous wave laser of 488 nm wavelength is incident to excite Raman signals from a sample. The power density of laser was measured to be 2.5×10^3 kW/cm^2 at the focus spot. In order to make an evanescent excitation light at the focus spot to improve Raman measurement, a mask is inserted in the entry of an expanded laser beam (pass NA > 1 and reject NA < 1).[29] To detect Raman scattering, an edge filter is used to reject Rayleigh scattering. A specific Raman line is selected by a spectrometer and then detected by an avalanche photodiode (APD). For the purpose of detecting Raman intensity at different tip-sample distance, a multichannel photon counter (NanoHarp 250, PicoQuant) is utilized. It is synchronized with the trigger signal supplied for tapping oscillation of AFM and it counts the Raman intensity signal. Through the multichannel photon counter, time-correlated Raman measurement is implemented. Since the tapping oscillation is sinusoidal as shown in the top graph of figure 4.2.1(b), tip-sample distance (D(t)) varies

with time. If tapping oscillation time is divided into many small time channels, a discrete time channel (Δt) shown in the middle graph of figure 4.2.1(b) can be set to the corresponding tip-sample distance. Therefore, the maximum tip-sample distance (D_{max}) can be known at the peak position of the sinusoidal curve and the minimum tip-sample distance (D_{min}) can be known at the valley position of the sinusoidal curve. In one tapping period, there are 64 sequential time channels as shown in the middle graph of figure 4.2.1(b). In our AFM, the tapping period is about 8 μs meaning each time channel is about 0.128 μs. For the time-correlated records of Raman intensity, the photon counter counts the number of photons within each time channel as shown in the bottom graph of figure 4.2.1(b). Due to distance dependence of the enhanced field, we can expect an intensity peak rests at the position of the minimum tip-sample distance as shown in figure 4.2.1(b). To get a certain amount of counts, we set the acquisition time to be 1 second in one tapping period.

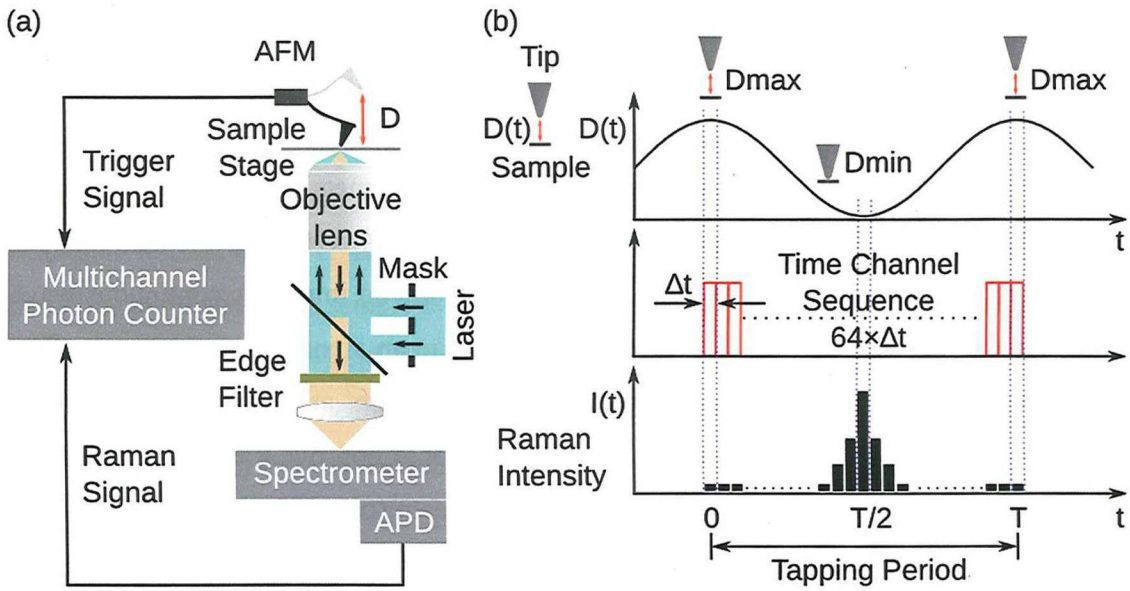

Figure 4.2.1 (a) Experimental setup for tip-enhanced near-field Raman microscopy through tapping-mode AFM configuration. (b) Schematic of time-correlated photon counting for Raman measurement.

In our experiments, single-walled carbon nanotubes (SWNTs) purchased from Meijo Nano Carbon Co., Ltd. are used as the sample. SWNTs are particular one-

dimensional structure that is directly linked to characteristic Raman bands. The diameter of a SWNT is 1.4 nm, which specifically suitable for demonstration of high spatially resolving power of TERS microscopy. Bundles of SWNTs with height of a few nanometers confirmed in AFM images were first sparsely spin-coated onto a glass coverslip. And then they were baked to remove any contaminations in an oven at the temperature of 300°C for 4 h. G mode of Raman scattering is selected for the imaging of SWNTs. G mode is originated from planar vibrations of carbon atoms in SWNTs. The Raman peak is found at the wavenumber of 1595 cm^{-1} in our experiments and a spectral width of 22 cm^{-1} is gated to pass into the APD. The photon signal is then recorded by the multichannel photon counter in synchronization with the tapping oscillation.

Commercial cantilevers (SI-DF20, Seiko Instruments Inc.) are evaporated with Ag nanoparticle layer to induce enhancement at the tip apex. The diameter of tip apex is about 30 nm after Ag evaporation, which is confirmed in scanning electron microscopy images. In our experiments, we carefully chose to use Ag-coated tip with an underlayer of SiO_2 instead of Si that is generally used in cantilever of AFM. Since the smaller refractive index of SiO_2 comparing to Si makes shift of the plasmon resonance wavelength of SPPs to our excitation wavelength of 488 nm,[30] resonant excitation of SPPs is achievable. By this treatment, a larger enhancement of Raman intensity can be achieved.

4.3 Tip-sample distance dependence of TERS

As a result, figure 4.3.1(a) illustrates a data of time-correlated Raman intensity measurement obtained while an Ag-coated nanotip is tapping on top of SWNTs. A distinct sharp peak at position A indicates that the tip is at the minimum tip-sample distance (D_{min}) as the enhanced field is the strongest at the minimum tip-sample distance. Because the tip does periodical oscillation, the position of the maximum tip-sample distance (D_{max}) can be found at the time that is half an oscillation period away from position A. It is marked at position B in figure 4.3.1(a). In tapping-mode AFM, the maximum tip-sample distance can be obtained by force curve measurement[26, 31] and it is

found to be around 113 nm in this experiment. Since each time corresponds to a specific tip-sample distance in figure 4.3.1(a) and the correlation between time and distance is sinusoidal, thus time-correlated Raman intensity can be converted into tip-sample distance dependent Raman intensity. In half a period, the time from position A to position B in figure 4.3.1(a) is converted into tip-sample distance. Figure 4.3.1(b) represents tip-sample distance dependent Raman intensity after conversion. It shows the trend of increasing intensity at short tip-sample distance, which indicates the great enhanced near-field signal in the vicinity of tip apex.

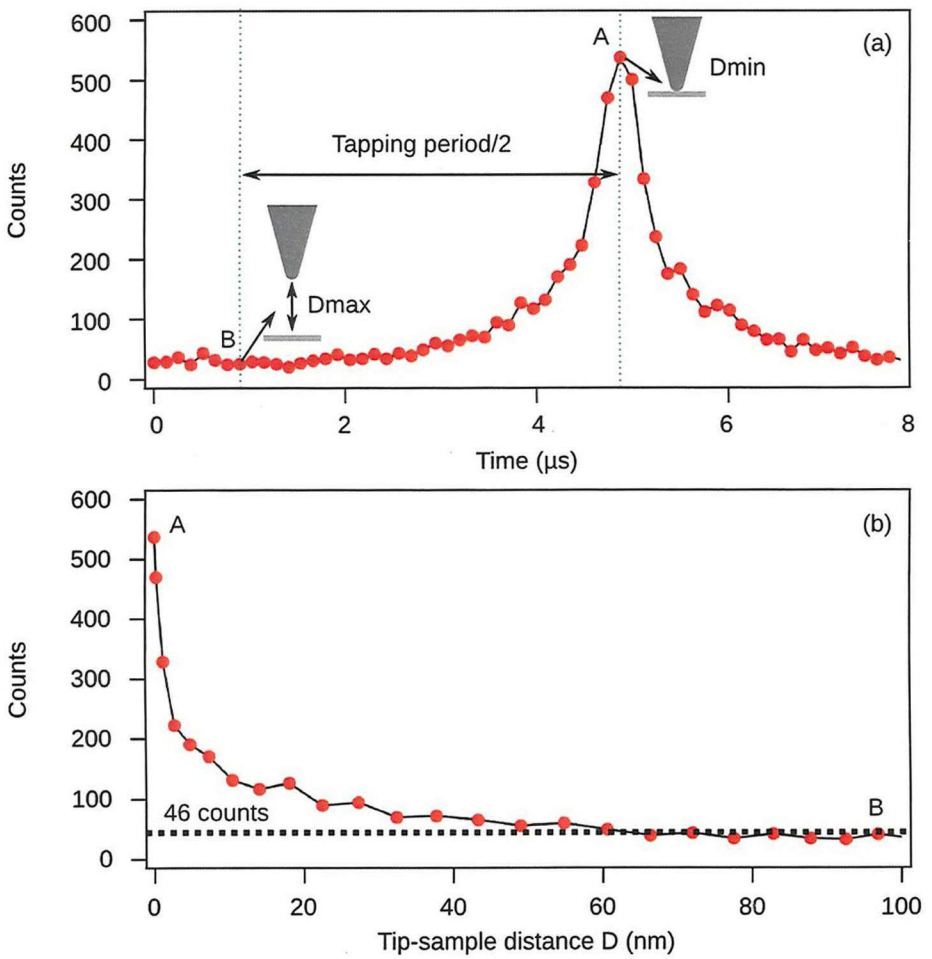

Figure 4.3.1 (a) Time-correlated Raman intensity measured while an Ag-coated nanotip is tapping on top of SWNTs. (b) Tip-sample distance dependent Raman intensity converted from position A to position B in graph (a).

Moreover, figure 4.3.1(b) also indicates that a constant level of far-field signal is about 46 counts as the dashed line shows. To make sure the far-field signal is detected, the background of APD itself was also measured. It was found to be 80 counts/second meaning 1.25 counts/second/channel that was much smaller than the signal level of far-field. In this measurement, the enhancement factor of the enhanced field at the tip apex is estimated to be about 1487 in considering the diameter of the tip apex of 30 nm and the diameter of the focus spot of 174 nm.

4.4 In situ far-field signal removal in TERS imaging of single-walled carbon nanotubes

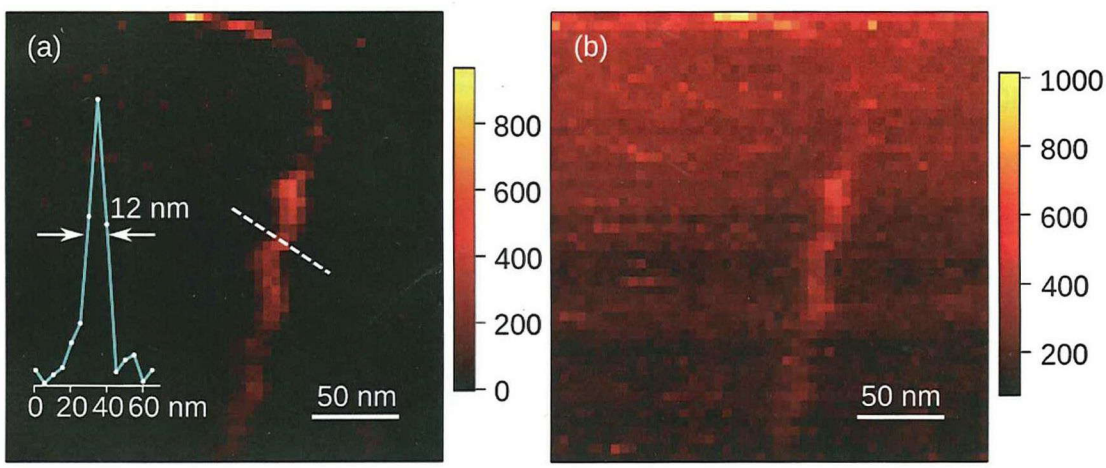

Figure 4.4.1 (a) Far-field free tip-enhanced Raman image of SWNTs. The inset graph is a cross section of SWNTs indicated by a dashed line. (b) Tip-enhanced Raman image with far-field signal. Both images have scan points of 50 × 50. The scale bar is 50 nm.

From tip-sample distance dependent Raman intensity, we can observe the decreasing of Raman signal as tip-sample distance increases, which represents the variation of the enhanced field near the tip apex. In our experiments, our data showed distinct enhanced near-field signal and constant level of far-field signal at different tip-sample distance. It is so convenient to get pure near-field signal by simply subtraction of far field signal. For the purpose of far-field free tip-enhanced Raman imaging, we did raster scanning of

sample stage at a scan step of 5 nm. Figure 4.4.1(a) displays a far-field free Raman image of SWNTs. At each scanning point, tip-sample distance dependent Raman intensity was measured and pure near-field signal was obtained in situ by subtraction. In contrast, a Raman image with far-field signal was constructed by using the intensity at the minimum tip-sample distance illustrated in figure 4.4.1(b). In comparison to figure 4.4.1(a), apparently far-field free image has better image contrast to show clear structure of SWNTs. Our method for tip-enhanced Raman imaging shows the power of in situ subtraction of far-field signal and has the advantage of one time measurement. Moreover, the far-field free Raman image demonstrates a resolution of 12 nm at full width half maximum (FWHM) from a cross section of SWNTs shown in the inset graph of figure 4.4.1(a). The white dashed line indicates the place where the cross section is

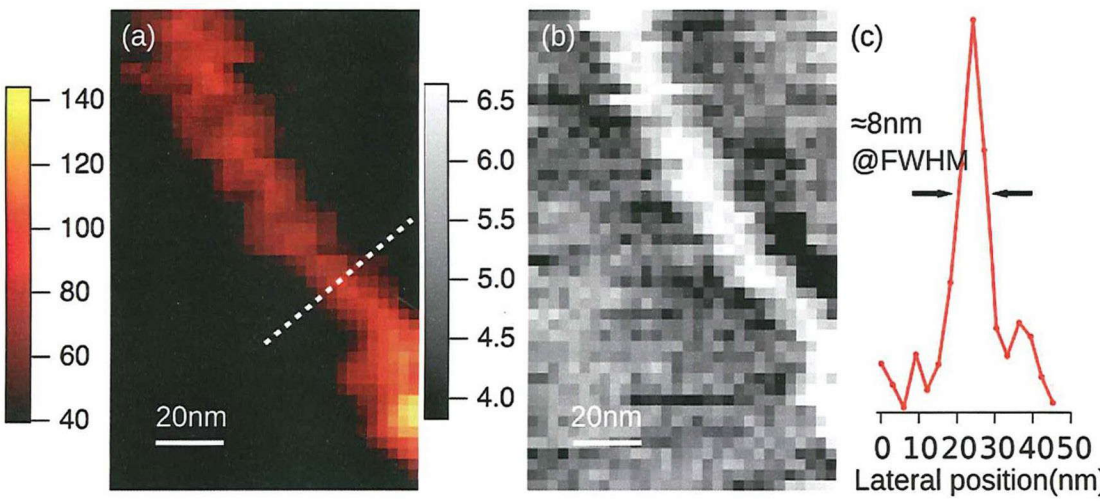

taken from.

Figure 4.4.2 (a) Far-field free tip-enhanced Raman image of SWNTs. (b) Simultaneously obtained AFM image. (c) Cross section of SWNTs indicated by the white dashed line in the Raman image. Both images have scan points of 30 × 45. The scale bar is 20 nm.

With the merit of in situ far-field subtraction, tapping-mode tip-enhanced Raman imaging can improve image contrast. In order to demonstrate its high-resolution power as well, we reduced the scan step to 3 nm. In figure 4.4.2(a), a tip-enhanced Raman

image after in situ subtraction of far-field Raman intensity is illustrated. In addition, figure 4.4.2(b) is a simultaneously obtained AFM image. In the AFM image, the height of the SWNTs is confirmed at around 2.8 nm, which means that it is a bundle of SWNTs. In figure 4.4.2(c), the cross section of SWNTs in the Raman image is illustrated. The value of FWHM of the cross section indicates that the spatial resolution of the Raman image reaches about 8 nm.

In summary, a tapping-mode TERS microscope is constructed and exhibits its appropriate efficiency of in situ far-field signal removal in TERS imaging. Due to tip-sample variation in tapping-mode AFM, it is easy to get tip-sample distance dependent Raman intensity, which is a proper way to evaluate the confinement property of different metallic nanotips. Furthermore, by using tapping-mode operation AFM, we can also avoid sample damage.[26,28] This is important for future application of TERS to soft biological materials where the tip force applied on the sample may cause critical deformations.

References

1. N. Hayazawa, T. Yano, H. Watanabe, Y. Inouye and S. Kawata, Chemical Physics Letters **376** (1-2), 174-180 (2003).
2. B. Pettinger, B. Ren, G. Picardi, R. Schuster and G. Ertl, Physical Review Letters **92** (9) (2004).
3. J. Stadler, T. Schmid and R. Zenobi, Nano Letters **10** (11), 4514-4520 (2010).
4. C. Georgi and A. Hartschuh, Applied Physics Letters **97** (14) (2010).
5. T. Deckert-Gaudig, E. Rauls and V. Deckert, The Journal of Physical Chemistry C **114** (16), 7412-7420 (2010).
6. N. Jiang, E. T. Foley, J. M. Klingsporn, M. D. Sonntag, N. A. Valley, J. A. Dieringer, T. Seideman, G. C. Schatz, M. C. Hersam and R. P. Van Duyne, Nano Letters (2011).
7. A. Hartschuh, E. J. Sánchez, X. S. Xie and L. Novotny, Physical Review Letters **90** (9) (2003).
8. J. Steidtner and B. Pettinger, Physical Review Letters **100** (23) (2008).
9. T. Ichimura, S. Fujii, P. Verma, T. Yano, Y. Inouye and S. Kawata, Physical Review Letters **102** (18) (2009).
10. T.-a. Yano, P. Verma, Y. Saito, T. Ichimura and S. Kawata, Nature Photonics, 1-5 (2009).
11. P. Verma, T. Ichimura, T. Yano, Y. Saito and S. Kawata, Laser & Photonics Reviews **4** (4), 548-561 (2010).
12. B. Pettinger, P. Schambach, C. J. Villagómez and N. Scott, Annual Review of Physical Chemistry **63** (1), 379-399 (2012).
13. N. Hayazawa, Y. Inouye, Z. Sekkat and S. Kawata, Optics Communications **183** (1-4), 333-336 (2000).
14. M. S. Anderson, Applied Physics Letters **76** (21), 3130-3132 (2000).
15. R. M. Stöckle, Y. D. Suh, V. Deckert and R. Zenobi, Chemical Physics Letters **318** (1-3), 131-136 (2000).
16. B. Hecht, H. Bielefeldt, L. Novotny, Y. Inouye and D. W. Pohl, Physical Review Letters **77** (9), 1889-1892 (1996).
17. E. Hutter and J. H. Fendler, Advanced Materials **16** (19), 1685-1706 (2004).

18. C. Noguez, Journal of Physical Chemistry C **111** (10), 3806-3819 (2007).
19. E. Betzig, P. L. Finn and J. S. Weiner, Applied Physics Letters **60** (20), 2484-2486 (1992).
20. W. A. Atia and C. C. Davis, Applied Physics Letters **70** (4), 405-407 (1997).
21. I. Schmitz, M. Schreiner, G. Friedbacher and M. Grasserbauer, Analytical Chemistry **69** (6), 1012-1018 (1997).
22. A. Hartschuh, N. Anderson and L. Novotny, Journal of Microscopy **210** (3), 234-240 (2003).
23. L. G. Cançado, A. Hartschuh and L. Novotny, Journal of Raman Spectroscopy **40** (10), 1420-1426 (2009).
24. E. Bailo and V. Deckert, Chemical Society Reviews **37** (5), 921-930 (2008).
25. T. Yano, P. Verma, S. Kawata and Y. Inouye, Applied Physics Letters **88** (9) (2006).
26. T.-a. Yano, T. Ichimura, A. Taguchi, N. Hayazawa, P. Verma, Y. Inouye and S. Kawata, Applied Physics Letters **91** (12) (2007).
27. Q. Zhong, D. Inniss, K. Kjoller and V. B. Elings, Surface Science Letters **290** (1–2), L688-L692 (1993).
28. P. K. Hansma, J. P. Cleveland, M. Radmacher, D. A. Walters, P. E. Hillner, M. Bezanilla, M. Fritz, D. Vie, H. G. Hansma, C. B. Prater, J. Massie, L. Fukunaga, J. Gurley and V. Elings, Applied Physics Letters **64** (13), 1738-1740 (1994).
29. N. Hayazawa, Y. Inouye and S. Kawata, Journal of Microscopy **194** (2-3), 472-476 (1999).
30. A. Taguchi, N. Hayazawa, Y. Saito, H. Ishitobi, A. Tarun and S. Kawata, Optics Express **17** (8), 6509-6518 (2009).
31. C. Su, L. Huang and K. Kjoller, Ultramicroscopy **100** (3–4), 233-239 (2004).

Chapter 5.

Tip-enhanced fluorescence at optimized tip-sample separation

The enhancement and quenching induced by a metallic nanotip to fluorescence modify the strength of fluorescence in two completely opposite ways as expressed by their literal meanings. The influence of enhancement and quenching results a certain value of distance between tip and fluorophore for the strongest value of field or fluorescence. High-quality tip-enhanced fluorescence nano-imaging is expected at the certain distance. To determine the certain distance, an approach of regulating tip-fluorophore separation is required. It is developed by utilizing the tapping operation of atomic force microscopy. In this chapter, firstly the fluorescent sample (quantum dot) is introduced and the reason for sample selection is described; next the experimental way of controlling tip-sample separation to obtain strongest strength of fluorescence is explained and then some results are presented for discussion.

5.1 Quantum dot and its properties

Quantum dots are semiconductor nanocrystals whose radii are smaller than the critical characteristic length called exciton Bohr radius (a few nanometers).[1, 2] They are fluorescent and have high quantum yields (30%~80%).[3, 4] In quantum dots, energy levels are quantized and their values are directly related to the size. As size is reduced, the electronic excitations shift to higher energy and the exciton (electron-hole pair) strength is concentrated into just a few transitions. These basic physical phenomena of

quantum confinement arise as a result of changes in the density of electronic states.[1] Quantum confinement makes quantum dots exhibit strongly size-dependent optical and electronic properties. By a method of chemical synthesis, size of quantum dots can be precisely controlled.[5-8] This helps to easily tune their optical and electronic properties for different applications.[5, 9, 10] In practice, the radiative recombination of excitons lead to fluorescence emission in a narrow and symmetric shape. Comparing to many other biological fluorescent molecules, fluorescence from quantum dots has a longer lifetime characterized as ~10 ns. Surface defects in quantum dots usually act as temporary "traps" for the electron or hole, preventing their radiative recombination. This reduces the overall quantum yield and causes intermittent fluorescence. To solve this problem, a shell of a few atomic layers of a material with a larger band gap is used to encapsulate the quantum dot core. It can protect surface atoms from oxidation and other chemical reactions. The core-shell structured quantum dots show much better photostability and higher quantum yield.[5]

In the study of tip-enhanced fluorescence microscopy, quantum dots become an ideal fluorescent sample. The size of a few nanometers is small enough to demonstrate the high resolving power in tip-enhanced fluorescence microscopy. In addition, the wide range of absorption in visible light facilitates to choose an excitation laser having a resonant plasmonic wavelength of the metallic nanotip. Moreover, the photostability of quantum dots helps us to determine the only possibility of fluorescence quenching from the metallic nanotip.

In the experiments, commercial quantum dots purchased from NN-LABS, LLC are used as fluorescent samples. The quantum dot is a core/shell structure with CdSe as the core and ZnS as the shell. The CdSe core has a diameter of ~6.2 nm and the ZnS shell has a thickness of ~1.7 nm. Figure 5.1.1 shows the absorption and fluorescence emission spectra of the quantum dots. The absorption spectrum depicted by red color is measured by white light illumination. It illustrates that the quantum dots have an absorption peak at about 640 nm. The absorption of 640 nm light indicates that this light energy equals to the energy of transition from ground state to the first order excited electronic state, which is the energy band gap of CdSe. The absorption spectrum also shows an increased absorption in the shorter wavelength as a result of direct absorption

into the higher band gap ZnS shell.[5] The fluorescence emission spectrum depicted by blue color is measured when quantum dots are excited by a laser light of 488 nm wavelength. It shows a strong peak at 640 nm, which is the very energy band gap between the first order excitation electronic state and ground state in CdSe core. The small peak of 488 nm is from excitation laser after an edge filter.

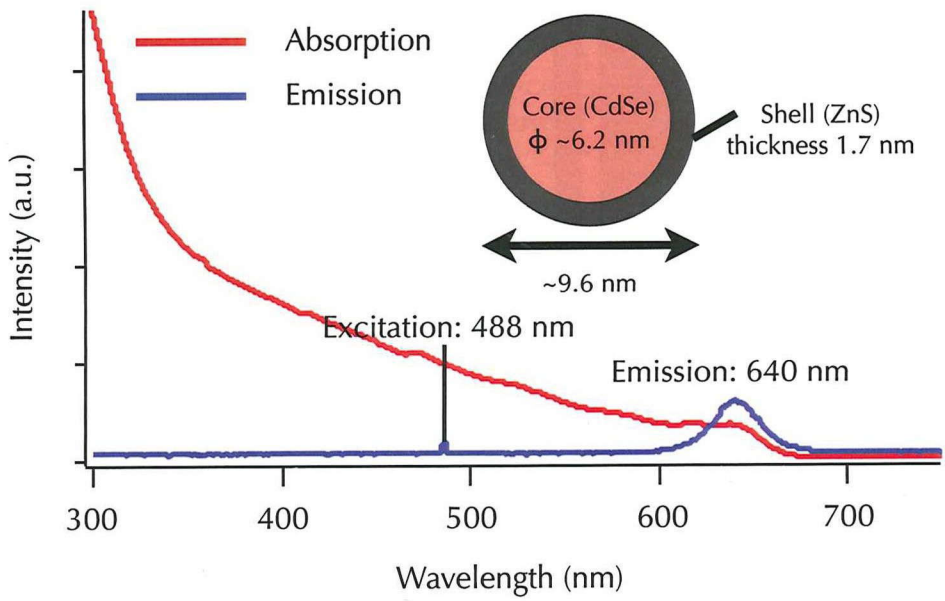

Figure 5.1.1 Absorption (red color) and fluorescence emission (blue color) of quantum dots. The schematic illustration shows the core/shell structure of a quantum dot.

The core/shell quantum dots are preserved at a high concentration in toluene solvent to protect and stabilize the unique optical properties of the quantum dots from damaging environmental effects. In order to detect tip-enhanced fluorescence from isolated quantum dots in a diffraction-limited area, quantum dots solution needs to be extremely diluted (by adding 5000 times additional toluene). The diluted quantum dots are then spin-coated onto a clean cover glass at a speed of 2000 rotation/minute. To confirm single quantum dots are prepared, an AFM image and a far-field fluorescence image of the same sample are obtained as shown in Figure 5.1.2. In an area of 5 μm × 5 μm, several single quantum dots marked by circles are isolated to each other. The height of quantum dots measured in the AFM image is around 6 nm, indicating single quantum dots are prepared. The error of height is probably caused by AFM system without

precisely calibration. Comparing to the fluorescence image at the same places, they have spatially isolated fluorescence emission signals. Such a sample is then suitable for us to do analysis of enhancement and quenching in tip-enhanced fluorescence.

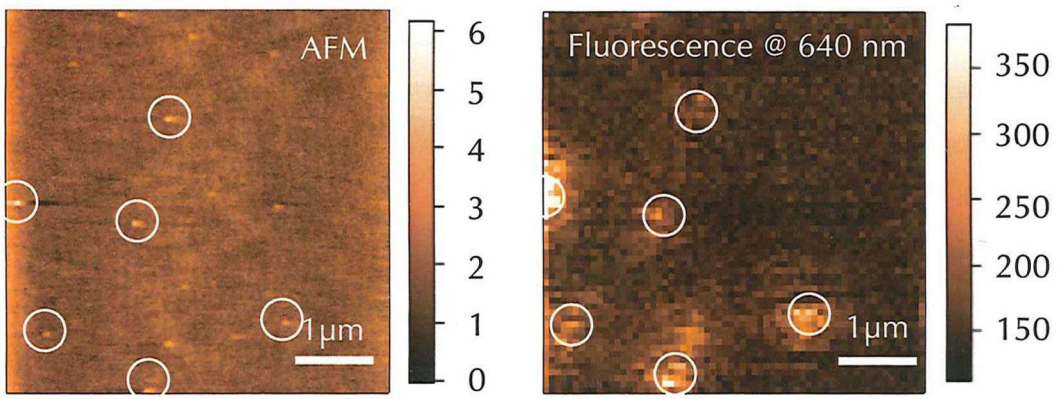

Figure 5.1.2 AFM image (left) and far-field fluorescence image (right) of quantum dots. Fluorescence image is constructed from emission intensity at 640 nm. The color bar of AFM image indicates height information in nm. The color bar in the fluorescence image indicates intensity information in arbitrary unit.

5.2 Tapping-mode tip-enhanced fluorescence microscopy

In conventional tip-enhanced fluorescence microscopy, a dielectric or metallic nanotip is maintained at a certain distance (0~7 nm) from the fluorescent sample in contact mode atomic force microscopy (AFM) or shear force microscopy, respectively.[11-16] As we mentioned in Chapter 2, quenching is dominant in such a short distance, imaging quality could be severely influenced. In contrast, tapping mode AFM exhibits an advantage to control tip-sample distance and determine the optimized distance for fluorescence imaging. Tip-enhanced fluorescence microscopy at 10 nm resolution has been reported by utilizing tapping-mode AFM.[17, 18] The efficient removal of far-field background was demonstrated to optimize fluorescence imaging. However, quenching was not observed in these studies because the authors used a silicon tip that does not quench fluorescence. In our study, a silver-coated AFM tip is used in order to observe

both enhancement and quenching and find out the optimized tip-sample distance for fluorescence imaging.

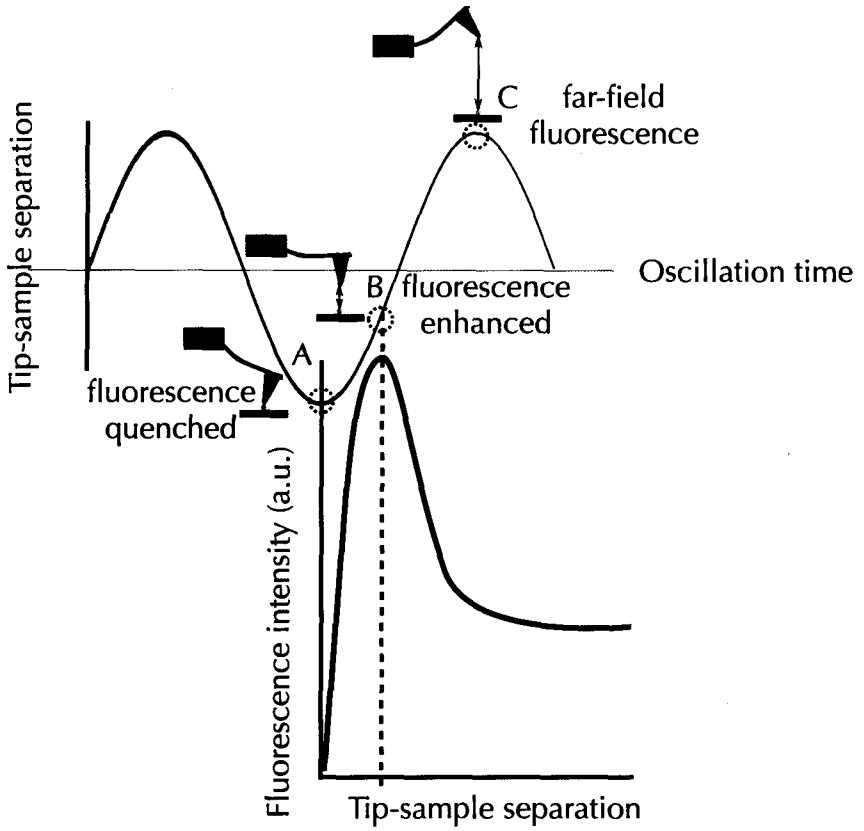

Figure 5.2.1 Schematic illustration of measuring tip-sample separation dependent fluorescence intensity

The control of tip-sample distance is realized in tapping mode AFM. And synchronization of tapping oscillation and time-gated photon detection leads to obtain tip-sample distance dependent fluorescence intensity. Figure 5.2.1 schematically illustrates this process. The sine wave at the top of the figure represents variation of tip-sample separation as a function of oscillation time. The frequency of tip-sample separation oscillation is the same as the driven signal for tip oscillation. It is determined by Q curve measurement in advance. Three positions of A, B, C on the sine wave mean three different tip-sample separations in an increasing direction. With synchronization of tapping oscillation and time-gated photon detection, fluorescence intensity of different tip-sample separations can be obtainable. Previous theoretical calculation

demonstrated a curve of fluorescence intensity as a function of tip-sample separation.[19] It is illustrated as the red curve shown at the bottom of figure 5.2.1. The competition of enhancement and quenching results peak intensity at position B. It indicates that the tip-sample separation at position B is the optimized separation for fluorescence imaging. At position A, because tip contacts the sample, fluorescence is quenched to disappear. At position C, only far field fluorescence is detected due to the enhanced field at the metallic tip is far way from the sample. Since intensity at position A (I_A) is enhanced signal superimposed on the far-field background signal at position C (I_c), in situ far-field subtraction can be efficiently implemented by I_A-I_B.

For tip-enhanced fluorescence microscopy at the optimized tip-sample separation, raster scanning of sample stage is applied through AFM. At each scanning point, the tip-sample separation dependent intensity is measured and in situ far-field subtraction can be carried out. Hence the intensity after subtraction of far-field signal at the optimized tip-sample is obtained to construct a fluorescence image.

5.3 Experimental setup

The experimental setup is illustrated in figure 5.3.1. It is based on an inverted oil-immersion optical microscope integrated with a tapping-mode AFM. An objective lens with numerical aperture (NA) of 1.4 is used to improve the ability to collect light and resolve the sample. The sample stage is controlled by piezos and can be raster scanned to obtain an image. Sample is spread on the glass substrate, where a tapping tip is above. A continuous wave laser of 488 nm wavelength is incident to excite fluorescence from quantum dots. The power density of laser was measured to be 4 kW/cm^2 at the focus spot, which is not strong enough to cause damage on quantum dots. In order to make evanescent excitation at the focus spot to improve fluorescence measurement, a mask is inserted in the entry of an expanded laser beam (pass NA > 1 and reject NA < 1). Fluorescence from the sample is recollected by the objective lens and guided to a band filter (center wavelength 640 nm, FWHM 40 nm). After a focusing system, fluorescence intensity is detected by an avalanche photodiode (APD). For the purpose of detecting fluorescence intensities at different tip-sample separation, a multichannel photon

counter (NanoHarp 250, PicoQuant) is utilized. It is synchronized with the trigger signal supplied for tapping oscillation of AFM and it counts the fluorescence intensity signal. Through the multichannel photon counter, time-correlated fluorescence measurement is implemented.

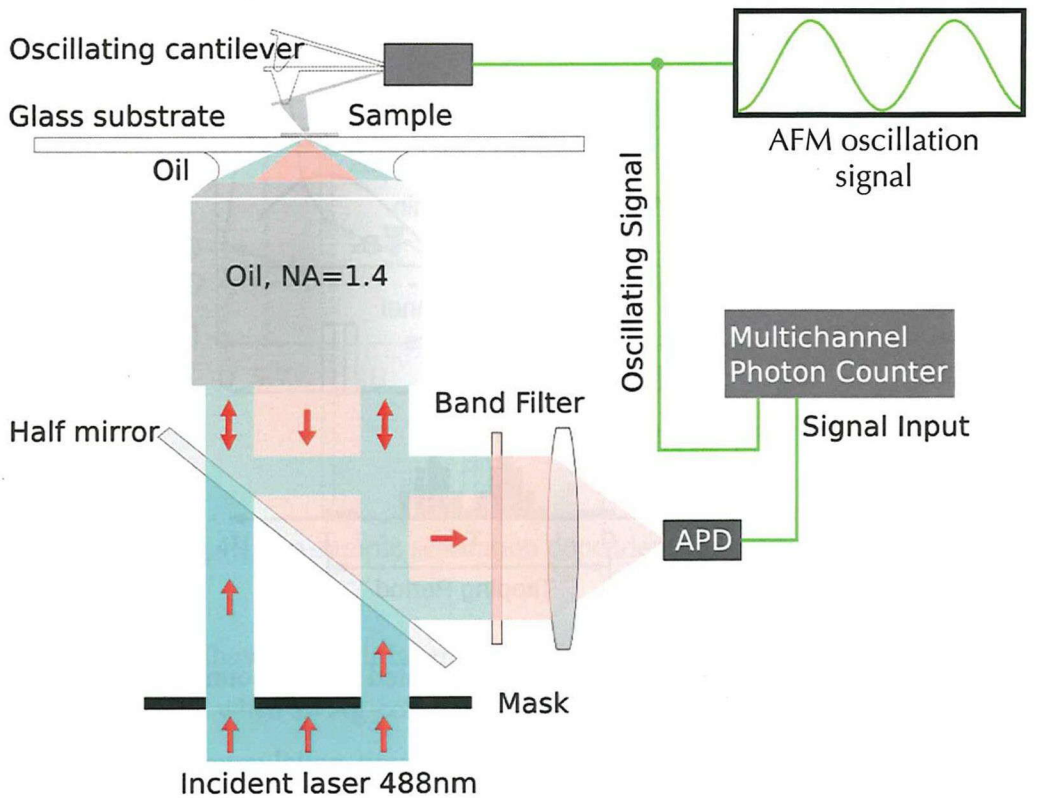

Figure 5.3.1 Schematic illustration of experimental setup

Experimentally, time-correlated photon counting is carried out in multichannel photon counter and then the time is converted to tip-sample separation. Time-correlated photon counting is illustrated in figure 5.3.2. The top graph of figure 5.3.2 describes the sinusoidal relation between tip-sample separation (D(t)) and time (t). In one tapping period (T), 64 sequential time channels (Δt) are set to gate optical signals. Thus each time channel corresponds to a tip-sample separation as marked by dotted lines, such like maximum tip-sample separation (D_{max}), minimum tip-sample distance (D_{min}) and optimized tip-sample distance (D_x). In our AFM, the tapping period is about 8 μs meaning each time channel is 0.128 μs. For the time-correlated records of fluorescence intensity, the photon counter counts the number of photons within each time channel as

shown in the bottom graph of figure 5.3.2. Due to tip-sample separation dependence of enhancement and quenching, there is an intensity peak sitting at D_x. And due to the dominant quenching effect, fluorescence intensity should be very weak at D_{min}. Therefore, time-correlated fluorescence intensity in a period is expected to have two peaks as shown in the bottom graph of figure 5.3.2.

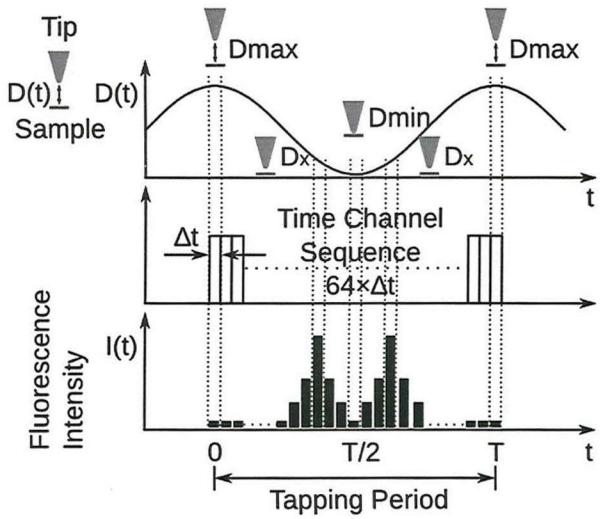

Figure 5.3.2 Schematic of time-correlated photon counting

The imaging process is carried out by scanning sample stage after the metallic tip is moved to the center of focus spot of laser light.

5.4 Tip-sample separation dependence of enhancement and quenching in fluorescence

A metallic tip in the vicinity of a fluorophore can lead to significant modifications to the radiative decay rate, nonradiative decay rate as well as quantum yield.[20-22] As a consequence, either enhancement dominance or quenching dominance of fluorescence has been reported.[11, 12, 14-16, 19, 23-28] The results greatly depend on the distance between the tip and the sample. In order to observe the transitional modification of fluorescence strength caused by enhancement and quenching, tip-sample separation dependent

fluorescence intensity needs to be measured. In our experiments, the transitional modification of fluorescence strength is obtained by an approach of time-gated photon counting synchronized with tapping oscillation of an Ag-coated nanotip.

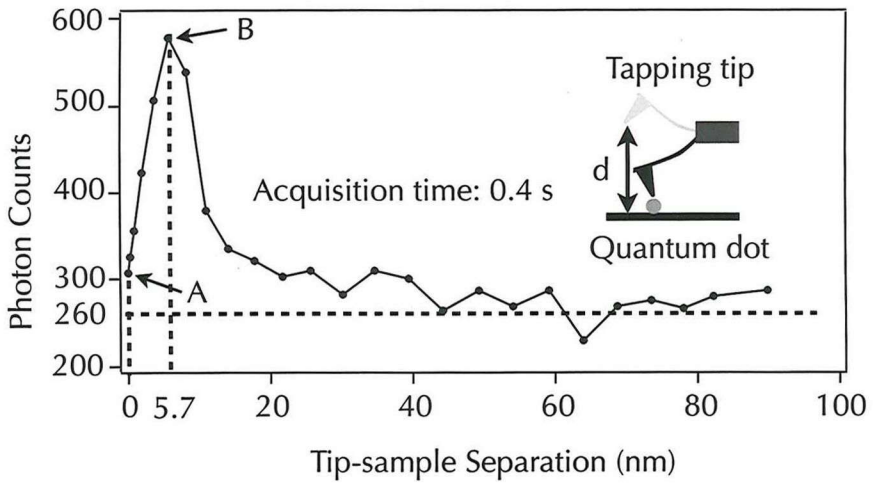

Figure 5.4.1 Tip-sample separation dependent fluorescence intensity

Figure 5.4.1 shows a result taken by our experimental setup shown in figure 5.3.1. The result is taken when an Ag-coated tip is tapping on top of a single quantum dot. It is acquired in an accumulation time of 0.4 s, which is about 5×10^4 cycles of tapping oscillation. The tip-sample separation is converted from time according to the sinusoidal relation explained in Chapter 3. In this result, both quenching and enhancement effects of Ag-coated tip on fluorescence intensity is obviously presented. In the short-range of tip-sample separation (< 5.7 nm), the quenching is dominant over enhancement, thus it is a drop of intensity (photon counts) with decreasing tip-sample separation. As tip-sample separation goes larger till 30 nm, quenching gradually decreases its effect, and enhancement is dominant over it, thus it is a lift of intensity (photon counts) with decreasing tip-sample separation. Finally, tip-sample separation goes much large (> 30 nm) to separate the tip from the sample far enough, that makes no enhanced field to enhance fluorescence, and thus far-field fluorescence intensity is detected to have an averaged level around 260 counts. In this result, tip-sample separation of 5.7 nm is found to be the optimized value for the optimization of tip-induced quenching and enhancement.

The enhanced intensity is about 2.2 times larger than the far-field level in this experiment. Comparing to the enhancement of Raman scattering from the similar Ag-coated tip, the enhancement is not so strong. This is probably due to plasmonic enhancement having much more resonant effect on Raman scattering than on fluorescence. Because the wavelength of Raman scattering is much closer to the resonant excitation wavelength of 488 nm than the emission wavelength of fluorescence of 640 nm.

5.5 Fluorescence imaging at optimized tip-sample separation

Tip-enhanced fluorescence microscopy has been demonstrated its ability of imaging specimen at a resolution of a few tens of nanometers. It is benefited from the confinement and enhancement of the light field at the apex of a metallic nanotip. The near-field tip-enhanced fluorescence image is obtained by the typical raster-scanning technique used in scanning probe microscopy. To date, tip-enhanced fluorescent images of quantum dots,[16, 17, 30] single molecules,[19, 31] and DNA[18] have all been reported. However, the obtained tip-enhanced fluorescence images were not the result of the optimization of quenching and enhancement. Quenching of fluorescence was purposely decreased or removed by some methods in these studies, which is attributed to the increasing possibility of energy transferring from fluorophore to metal,[32-35]. For example, dielectric tips were used to decrease effect of quenching,[12, 17, 36] in other ways, an interval layer was added or a certain distance was maintained between a metallic tip and a sample to prevent the metallic tip from directly contacting with the sample.[11] The ways of removing quenching somehow compromise losing of enhancement if the certain distance is not optimized. Our study provides a way to overcome this problem by finding the optimized tip-sample distance for tip-enhanced fluorescence imaging. In addition, in situ subtraction of far-field signal is efficiently achieved as explained in section 5.2.

To specifically detect the only quenching caused by the metallic tip, quantum dots are used as the sample for their high photostability. Figure 5.5.1 shows a tip-enhanced fluorescence image and a topographic AFM image of the sample quantum dots. The

fluorescence image is constructed from fluorescence intensity at a tip-sample separation (d) of 0 nm. It is a far-field free image (far-field fluorescence intensity is subtracted). The tip-sample separation dependent intensity measured at position "A" of fluorescence image is illustrated at the bottom left. The acquisition time is 1 second. The AFM image shows the structural information of quantum dots. The line profile of the dotted line is illustrated at the bottom right, indicating heights of 9 nm and 20 nm. Since a single quantum dot has a height of ~9.6 nm, and the diameter of tip apex is about 50 nm, thus a few quantum dots are aggregated in this sample.

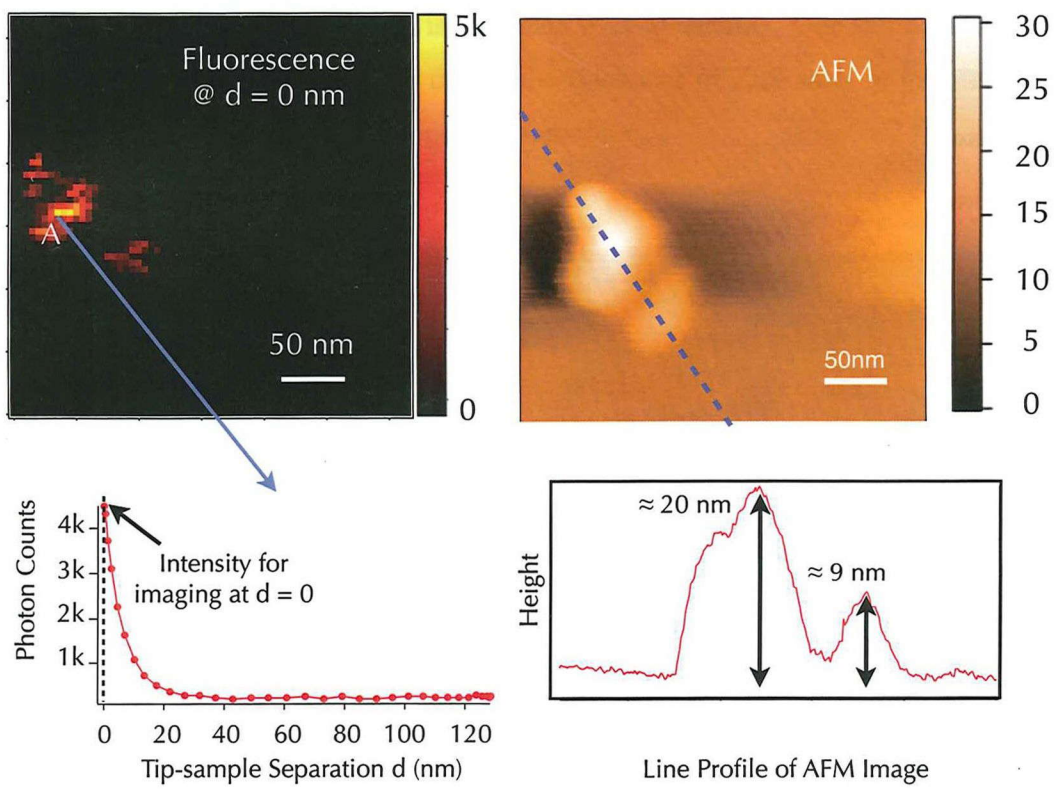

Figure 5.5.1 Tip-enhanced fluorescence image (top left) and AFM image (top right) of the same quantum dots. The scale bar is 50 nm in both images. Tip-sample separation dependent fluorescence intensity at position "A" in fluorescence image is illustrated in the bottom left. A line profile of sample depicted by the dashed line in AFM image is illustrated in the bottom right.

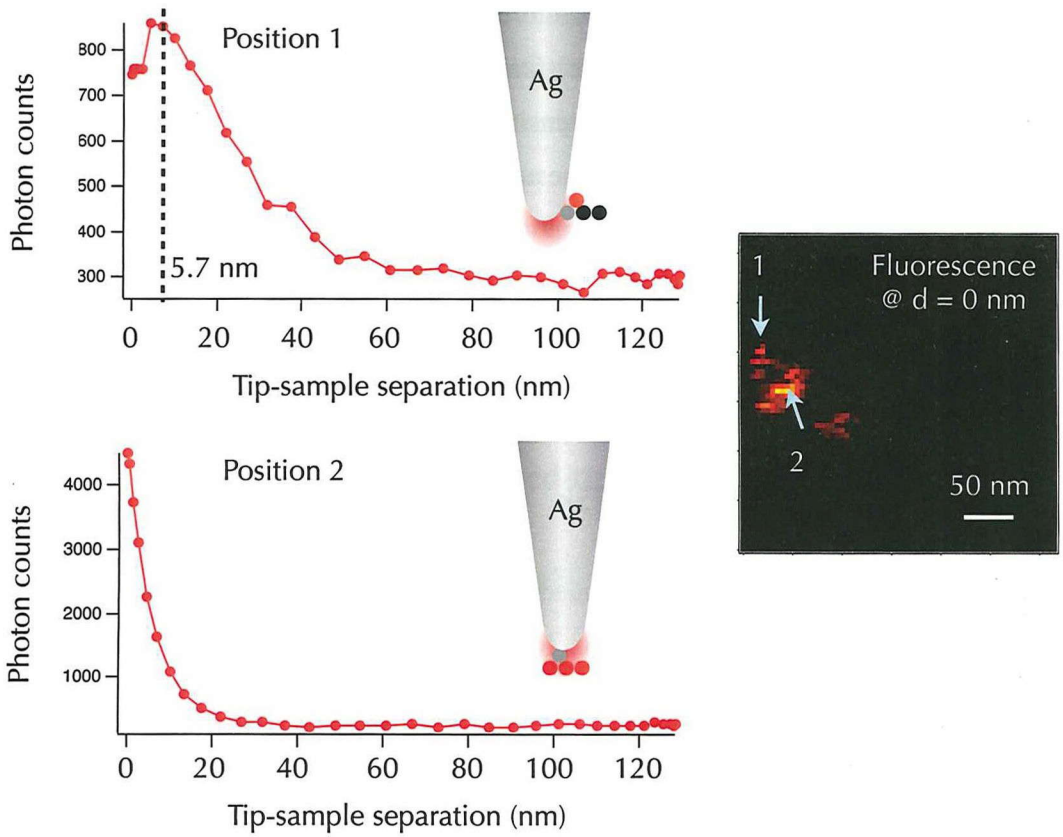

Figure 5.5.2 Tip-sample separation dependent fluorescence intensity at two different positions of the aggregated sample.

The tip-sample separation dependent fluorescence intensity in figure 5.5.1 shows enhanced intensity at very short tip-sample separations (< 20 nm). This indicates an enhanced field at the apex of Ag-coated tip. However intensity decreasing due to quenching is not observed at position "A". One possible reason is probably that the quantum dots are an aggregation, which makes the arrangement of tip and quantum dots very different. From the same fluorescence image, we analysis the tip-sample separation dependent intensity at different lateral positions of the sample. Figure 5.5.2 illustrates two tip-sample separation dependent curves on the left from two positions arrowed in the fluorescence image on the right. The tip-sample separation dependent intensity at position 1 shows a decreasing of intensity when the tip-sample separation is less than 5.7 nm. This indicates a quenching effect that is dominant over enhancement. In this occasion, the Ag-coated tip intermittently contacts with the sample at the edge region. It

can be described as the inset illustration. The red color represents the enhanced field at the apex of Ag-coated tip. Due to quenching is dominant when Ag-coated tip contacts with the quantum dots, and the effect of this enhanced field can only cover a single quantum dot (gray color) and other quantum dots (black color) are not excited by it, then a relative weak fluorescence strength can be detected at the short tip-sample separation (< 5.7 nm). In the other occasion shown at position 2, the Ag-coated tip intermittently contacts with the sample at the central region, where only enhancement is observed. The inset illustration describes one quantum dot is subjected to quenching effect while other three quantum dots (red color) are subjected to enhancement effect. Thus even in contact, enhancement is dominant over quenching. One another reason for the weak quenching effect may be due to the thickness of ZnS shell in quantum dots, which prevents quenching from happening sometime.

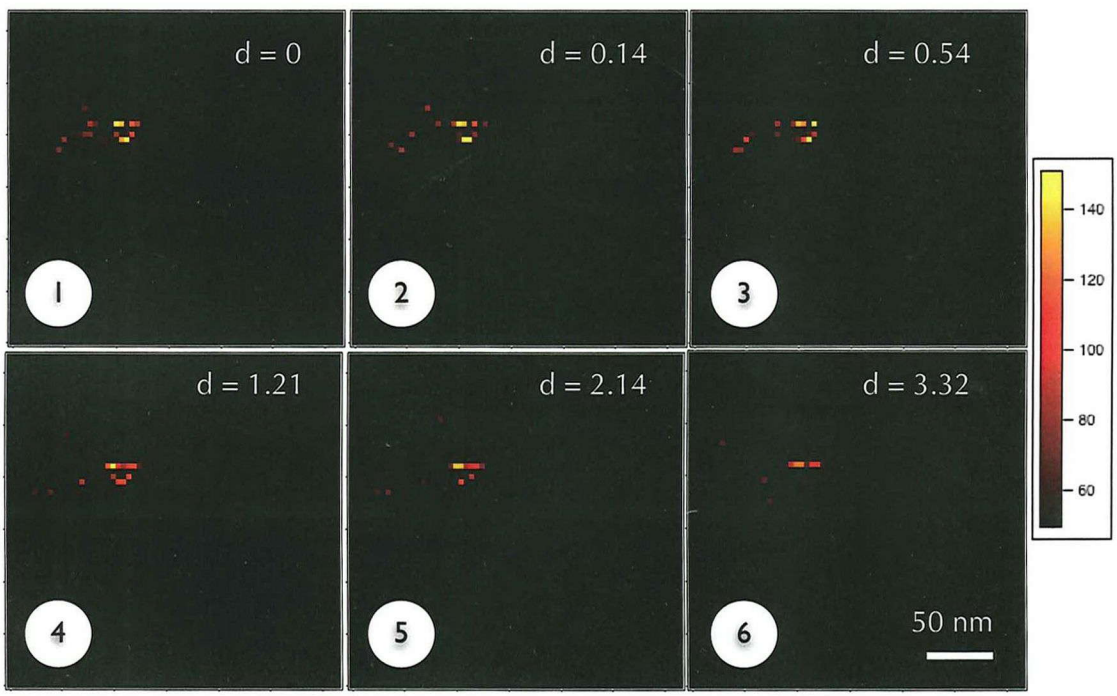

Figure 5.5.3 A group of fluorescence images of a single quantum dot at different tip-sample separations (d, unit: nm). The scale bar is 50 nm.

Since quantum dots aggregation complicates the variation of tip-sample separation dependent intensity, a sample of single quantum dot is preferable to determine the

optimized tip-sample separation for fluorescence imaging. In the experiment, an isolated single quantum dot was chosen for fluorescence imaging according the height information of AFM image. Figure 5.5.3 illustrates a group of fluorescence images that are constructed from the intensity at different tip-sample separations. These images show different structural shapes of quantum dot, indicating this quantum dot is an anisotropic structure. Probably the ZnS shell does not cover the CdSe core uniformly or there are several defects inside the quantum dot. The intensity data obtained in this experiment is not enhanced much comparing to the data obtained in figure 5.5.2, the reason is not only the smaller sample density but also the weaker light field from Ag-coated tip.

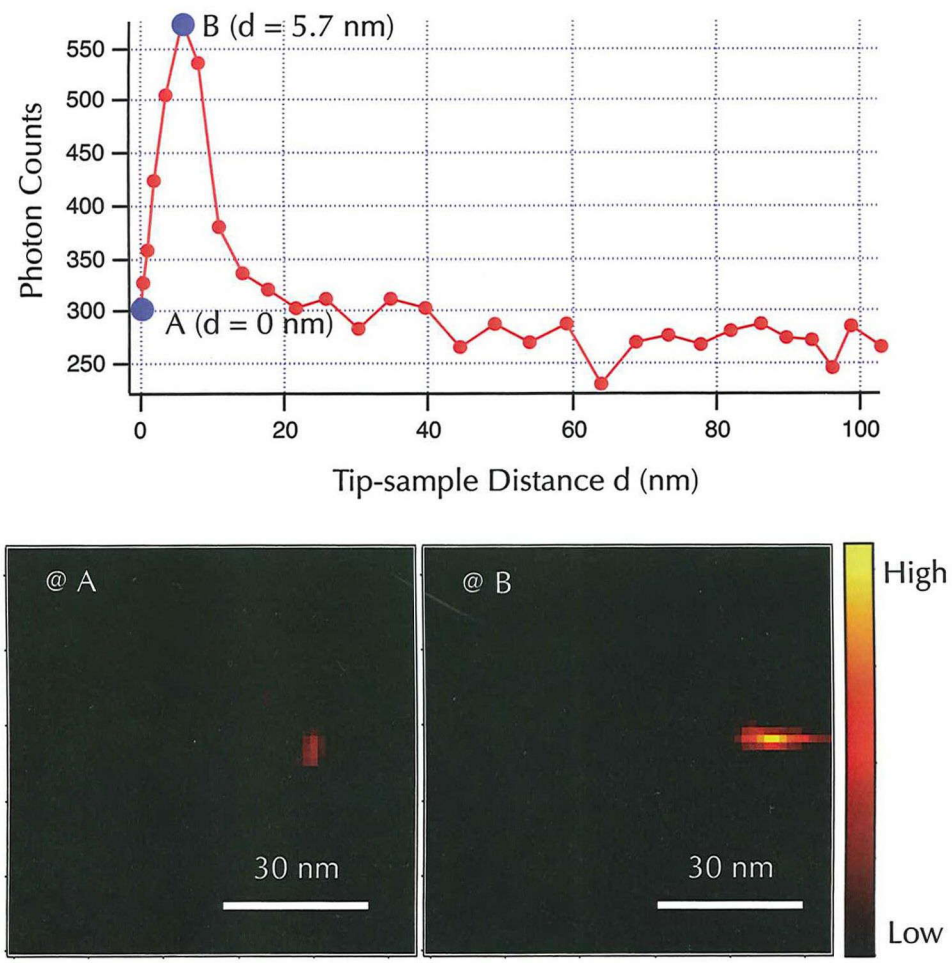

Figure 5.5.4 Comparison of tip-enhanced fluorescence imaging at different tip-sample separations. The scale bar is 30 nm.

Figure 5.5.4 demonstrates another result. In this result, an obvious variation of intensity caused by tip enhancement and tip quenching is observed as shown in the top graph. According to the variation of intensity, the optimized tip-sample separation is at B (5.7 nm). Thus an optimized tip-enhanced fluorescence image is obtained at tip-sample separation of 5.7 nm as shown in the bottom right. In contrast, an image at tip-sample separation of 0 nm is illustrated in the bottom left, which has weak fluorescence due to the quenching effect from the tip. Here the fluorescence in image @A is still observable that can be explained by the incomplete quenching from the hinder of ZnS shell. Obviously, image @B provides more structural information than image @A.

In summary, a few tip-enhanced fluorescence images are illustrated. All images are far-field free images benefitted from in situ far-field subtraction in our experiment technique. The enhancement and quenching induced by Ag-coated tip are observed in the tip-sample separation dependent fluorescence intensity. Fluorescence imaging at the optimized tip-sample separations of quantum dots is demonstrated as well.

References

1. A. P. Alivisatos, Science 271 (5251), 933-937 (1996).
2. X. Michalet, F. Pinaud, T. D. Lacoste, M. Dahan, M. P. Bruchez, A. P. Alivisatos and S. Weiss, Single Molecules 2 (4), 261-276 (2001).
3. A. M. Smith, H. Duan, M. N. Rhyner, G. Ruan and S. Nie, Physical Chemistry Chemical Physics 8 (33), 3895-3903 (2006).
4. S. F. Lee and M. A. Osborne, ChemPhysChem 10 (13), 2174-2191 (2009).
5. B. O. Dabbousi, J. Rodriguez-Viejo, F. V. Mikulec, J. R. Heine, H. Mattoussi, R. Ober, K. F. Jensen and M. G. Bawendi, The Journal of Physical Chemistry B 101 (46), 9463-9475 (1997).
6. C. B. Murray, D. J. Norris and M. G. Bawendi, Journal of the American Chemical Society 115 (19), 8706-8715 (1993).
7. M. A. Hines and P. Guyot-Sionnest, The Journal of Physical Chemistry 100 (2), 468-471 (1996).
8. C. J. Murphy, T. K. Sau, A. M. Gole, C. J. Orendorff, J. Gao, L. Gou, S. E. Hunyadi and T. Li, The Journal of Physical Chemistry B 109 (29), 13857-13870 (2005).
9. S. A. Empedocles, D. J. Norris and M. G. Bawendi, Physical Review Letters 77 (18), 3873-3876 (1996).
10. X. Michalet, F. F. Pinaud, L. A. Bentolila, J. M. Tsay, S. Doose, J. J. Li, G. Sundaresan, A. M. Wu, S. S. Gambhir and S. Weiss, Science 307 (5709), 538-544 (2005).
11. E. J. Sánchez, L. Novotny and X. S. Xie, Physical Review Letters 82 (20), 4014-4017 (1999).
12. H. F. Hamann, A. Gallagher and D. J. Nesbitt, Applied Physics Letters 76 (14), 1953-1955 (2000).
13. V. V. Protasenko, M. Kuno, A. Gallagher and D. J. Nesbitt, Optics Communications 210 (1-2), 11-23 (2002).
14. W. Trabesinger, A. Kramer, M. Kreiter, B. Hecht and U. P. Wild, Applied Physics Letters 81 (11), 2118-2120 (2002).

15. A. Kramer, W. Trabesinger, B. Hecht and U. P. Wild, Applied Physics Letters 80 (9), 1652-1654 (2002).
16. F. M. Huang, F. Festy and D. Richards, Applied Physics Letters 87 (18) (2005).
17. J. M. Gerton, L. A. Wade, G. A. Lessard, Z. Ma and S. R. Quake, Physical Review Letters 93 (18) (2004).
18. Z. Ma, J. M. Gerton, L. A. Wade and S. R. Quake, Physical Review Letters 97 (26) (2006).
19. P. Anger, P. Bharadwaj and L. Novotny, Physical Review Letters 96 (11) (2006).
20. J. Azoulay, A. Débarre, A. Richard and P. Tchénio, EPL (Europhysics Letters) 51 (4) (2000).
21. N. A. Issa and R. Guckenberger, Optics Express 15 (19), 12131-12144 (2007).
22. P. Bharadwaj and L. Novotny, Optics Express 15 (21), 14266-14274 (2007).
23. N. Hayazawa, Y. Inouye and S. Kawata, Journal of Microscopy 194 (2-3), 472-476 (1999).
24. L. T. Nieman, G. M. Krampert and R. E. Martinez, Review of Scientific Instruments 72 (3), 1691-1699 (2001).
25. T. J. Yang, G. A. Lessard and S. R. Quake, Applied Physics Letters 76 (3), 378-380 (2000).
26. S. Kühn, U. Hakanson, L. Rogobete and V. Sandoghdar, Physical Review Letters 97 (1) (2006).
27. E. Yoskovitz, D. Oron, I. Shweky and U. Banin, The Journal of Physical Chemistry C 112 (42), 16306-16311 (2008).
28. E. Shafran, B. D. Mangum and J. M. Gerton, Physical Review Letters 107 (3) (2011).
29. T.-a. Yano, T. Ichimura, A. Taguchi, N. Hayazawa, P. Verma, Y. Inouye and S. Kawata, Applied Physics Letters 91 (12) (2007).
30. C. Xie, C. Mu, J. R. Cox and J. M. Gerton, Applied Physics Letters 89 (14) (2006).
31. S. Kühn, U. H'akanson, L. Rogobete and V. Sandoghdar, Physical Review Letters 97 (1) (2006).
32. E. Yoskovitz, I. Hadar, A. Sitt, I. Lieberman and U. Banin, The Journal of Physical Chemistry C 115 (32), 15834-15844 (2011).

33. E. Dulkeith, A. C. Morteani, T. Niedereichholz, T. A. Klar, J. Feldmann, S. A. Levi, F. C. J. M. van Veggel, D. N. Reinhoudt, M. Möller and D. I. Gittins, Physical Review Letters 89 (20) (2002).

34. E. Dulkeith, M. Ringler, T. A. Klar, J. Feldmann, A. Muñoz Javier and W. J. Parak, Nano Letters 5 (4), 585-589 (2005).

35. P. P. Pompa, L. Martiradonna, A. D. Torre, F. D. Sala, L. Manna, M. De Vittorio, F. Calabi, R. Cingolani and R. Rinaldi, Nature Nanotechnology 1 (2), 126-130 (2006).

36. H. G. Frey, J. Paskarbeit and D. Anselmetti, Applied Physics Letters 94 (24) (2009).

Chapter 6.
Conclusions and outlook

Conclusions

This study focuses on the two competing processes of plasmonic enhancement and quenching in tip-enhanced fluorescence microscopy. For the purpose of achieving fluorescence nano-imaging beyond the diffraction limit, the plasmonic enhanced field is introduced to enhance fluorescence by a metallic nanotip. However, the very same metallic nanotip causes fluorescence quenching as well. Consequently, a new technique of controlling tip-sample separation needs to be developed to observe both enhancement and quenching. We describe that the effects on fluorescence of enhancement and quenching are dependent on the separation between tip and sample. The mutual competition between enhancement and quenching makes the strongest fluorescence intensity rest at an optimized tip-sample separation, typically ~6 nm. This is demonstrated from our experimental result of tip-sample separation dependent fluorescence intensity. At this optimized tip-sample separation, high spatial resolution fluorescence imaging is achieved.

The experimental technique to detect this optimized tip-sample separation is presented by utilizing tapping-mode atomic force microscopy (AFM) to realize tip-sample separation control. Through the synchronization of time-gated optical signal detection with tapping oscillation of AFM and conversion of time to tip-sample separation afterward, fluorescence intensity as a function of tip-sample separation is obtained. In addition, fluorescence intensity mapping at different tip-sample separation

can be realized with the raster scanning technique in AFM. This experiment technique for tip-sample separation control is applicable to tip-enhanced Raman microscopy as well. Results of Raman imaging of single-walled carbon nanotubes (SWNTs) are demonstrated. The spatial resolution reaches 8~12 nm. Since Raman scattering has no quenching effect from the metallic nanotip, the optimized tip-sample separation is 0 nm.

Another important aspect of our experimental technique is to carry out far-field free tip-enhanced optical imaging. With help of tip-sample separation control, far-field signal at the maximum tip-sample separation can be separated. Thus, a pure near-field optical image can be obtained by simply in situ subtraction of far-field signal. The obvious improvement of imaging resolution is demonstrated in our far-field free tip-enhanced Raman microscopy and tip-enhanced fluorescence microscopy.

Outlook

Although tapping-mode tip-enhanced fluorescence microscopy has demonstrated its great power to optimize enhancement and quenching by tip-sample separation control, we come to realize that this is strongly dependent on different sample. For quantum dots we used, the high photostability makes us to exclude other possible processes (e.g. photobleaching) of diminishing fluorescence. Then fluorescence quenching through energy transfer to metal nanotip is the only way we considered. But most fluorescent biomolecules are subjected to photobleaching under different environment. If many other processes happen to diminish fluorescence, it is hard to know at which tapping position tip is in contact with the sample. For further study on such samples, we need to find a way to distinguish the possibilities of decreasing of fluorescence intensity.

One way to know the contact tapping position is using Raman scattering. Because quenching does not happen in Raman scattering. By simultaneously detecting Raman scattering and fluorescence,[1] the precise tip-sample separation can be calculated for distance dependent Raman and fluorescence signals. Therefore, it is possible to analysis fluorescence intensity decreasing whether it is caused by tip quenching or other environmental factors.

Spectroscopy can actually provide more information of this tip-sample interaction. Instead of intensity detection, tapping-mode tip-enhanced optical microscopy can also be used to detect tip-sample separation dependent spectra. This can be realized by synchronizing laser illumination with tapping oscillation.[2] It can be more interesting to know the physical phenomenon behind the spectral variations in short-range tip-sample separations.

References

1. A. Hartschuh, H. N. Pedrosa, L. Novotny and T. D. Krauss, Science 301 (5638), 1354-1356 (2003).
2. T. Ichimura, S. Fujii, P. Verma, T. Yano, Y. Inouye and S. Kawata, Physical Review Letters 102 (18) (2009).

Appendix

Fabrication of Ag-coated tip

The metallic tip used in the experiments is Ag-coated. It is made from thermal evaporation of Ag nanoparticles on the commercial AFM tip. The commercial AFM tip is purchased from SII Nanotechnology (SI-DF20). Its characteristics are listed as below.

SI-DF20 cantilever
Material: Silicon
Oscillation frequency: 110~150 kHz
Radius of tip apex: 10 nm
Length of tip: 12.5 μm

The study of plasmonic resonant wavelength depending on SiO_2 thickness was done previously. It demonstrates that there is a blue shift of plasmonic resonant wavelength as the thickness of SiO_2 layer towards a large value.[1] This is shown in Figure 1. The calculation model is illustrated in the left of figure 1. The results of plasmonic resonant spectra with different thickness of SiO_2 are shown in the right of figure 1. To obtain great plasmonic enhancement at 488 nm excitation, the AFM tip is usually oxidized at 1100 Celsius degree for 15 minutes and then evaporated by Ag nanoparticles.

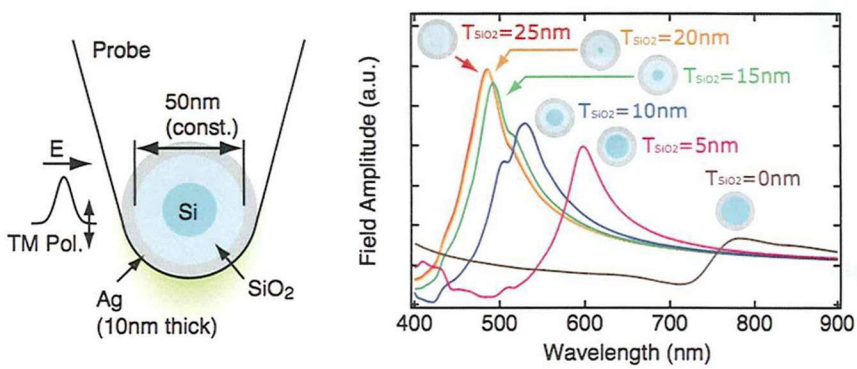

Figure 1. Calculation of SiO_2 thickness dependence of plasmonic resonant wavelength, referred from ref. 1

According to different vacuum degree and deposition rate, the result of Ag structures attached to the tip apex is very different. Figure 2 shows 4 scanning electron microscopy images of different tips, indicating a range of different diameters at the Ag-coated tip apex.

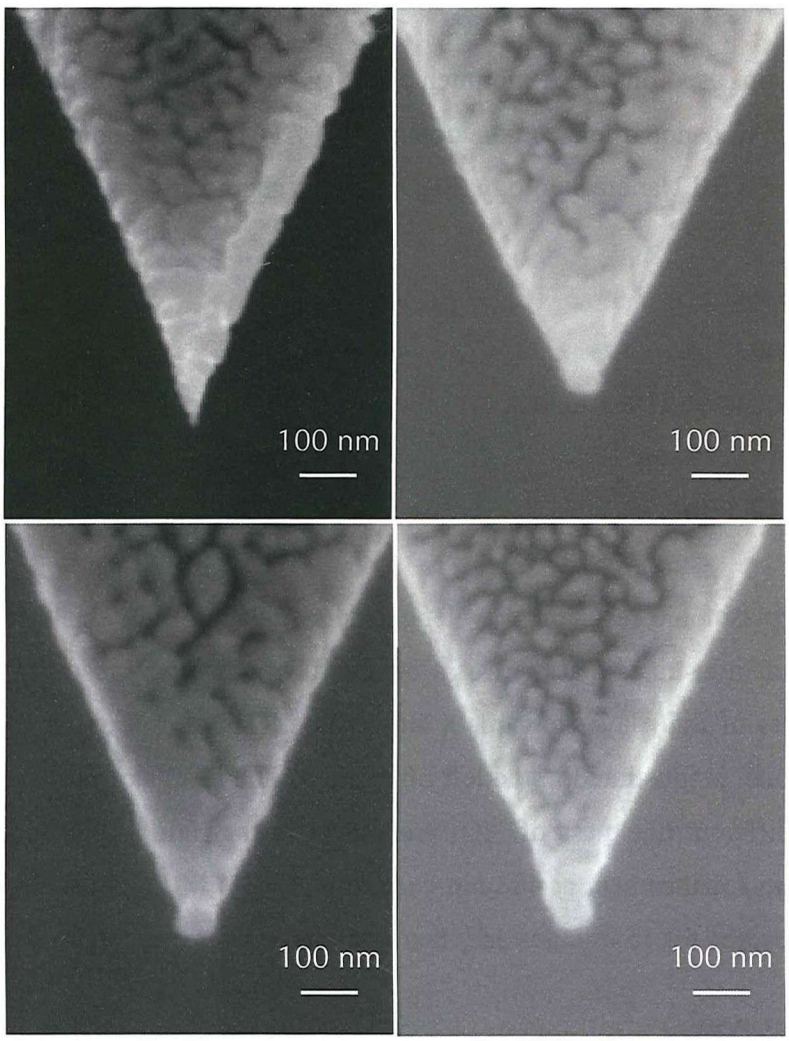

Figure 2 scanning electron microscopy images of Ag-coated tip

References

[1] A. Taguchi, N. Hayazawa, Y. Saito, H. Ishitobi, A. Tarun, and S. Kawata, Optics Express **17**, 6509 (2009).

Publications and conferences

Journal Papers

1. Jun Yu, Taro Ichimura, Yuika Saito, Satoshi Kawata, and Prabhat Verma "Far-field free tapping-mode tip-enhanced Raman microscopy", (Applied Physics Letters, submitted).

2. Jun Yu, Taro Ichimura, Yuika Saito, Satoshi Kawata, and Prabhat Verma "Tip-enhanced fluorescence microscopy at optimized tip-sample separation", (in preparation).

Conference Presentations

1. Jun Yu, Yuika Saito, Satoshi Kawata and Prabhat Verma, "Tip-enhanced Raman microscopy through tip-sample distance control", The 73rd JSAP Autumn Meeting 2012, JSAP-OSA Joint Symposia, Matsuyama, Japan, 2012.

2. Jun Yu, Taro Ichimura, Yuika Saito, Satoshi Kawata and Prabhat Verma, "Far-field free tapping-mode tip-enhanced Raman microscopy", The Seventh Photonics Center Symposium, Kanazawa, Japan, 2012.

Acknowledgments

This study is carried out under the supervision of Professor Satoshi Kawata and Professor Prabhat Verma in Laboratory for Scientific Instrumentation and Engineering (LaSIE), Department of Applied Physics, Osaka University. I would like to give them sincere thanks for their dedicated guidance and enlightening instructions. As a beginner of nano-optics, my supervisors not only guide me to catch every interest and brightness of this field, but also provide a great academic environment fully filled with wisdom and vigor. In this great academic environment, I have the chances to listen to interesting reports, learn knowledge, understand the science, think my own science, share ideas and communicate with many other members. My supervisors let me know that one should always think in a scientific way behind the phenomenon and be independent.

I would like to thank Professor Yoshihito Kobayashi and Professor Yasuhiro Sugawara who are both from Department of Applied Physics, Osaka University and Associate Professor Mamoru Hashimoto from Department of Mechanical Science and Bioengineering, Osaka University. They gave me many significant comments and suggestions during discussion of my study.

I am especially grateful to Dr. Taro Ichimura (Laboratory for Comprehensive Bioimaging, Riken Qbic) for his brilliant idea and help, letting me find a way to do this study. And thank to Associate Professor Yuika Saito, Assistant Professor Taka-aki Yano (Department of Electronic Chemistry, Tokyo Institute of Technology) and Dr. Katsumasa Uetsuki as well, they helped me a lot to carry out the experiments, fix problems and do scientific discussions. My gratitude also goes to Professor Yasushi Inouye, Associate Professor Katsumasa Fujita, Assistant professor Satoru Shoji, Dr. Almar F. Palonpon, Dr. Masahito Yamanaka, Dr. Kyoko Masui for available help in instruction, discussion and technical support.

In addition, I also would like to thank to all the members of NSOM group who contributed for every discussion and help of my work: Yoshito Okuno, Zhaoxu Yan,

Imad Maouli, Toshihiro Mino, Takayuki Umakoshi, Yshiro Ohashi. And thank all the LaSIE members for their great help about my study and life in Japan.

Finally, I would like to thank my wife for her devoted love and cares helping me finish my study.